TopBP1 is required at mitosis to reduce transmission of DNA damage to G1 daughter cells

Rune Troelsgaard Pedersen,[1] Thomas Kruse,[2] Jakob Nilsson,[2] Vibe H. Oestergaard,[1] and Michael Lisby[1]

[1]Department of Biology and [2]The Novo Nordisk Foundation Center for Protein Research, Faculty of Health and Medical Sciences, University of Copenhagen, DK-2200 Copenhagen N, Denmark

Genome integrity is critically dependent on timely DNA replication and accurate chromosome segregation. Replication stress delays replication into G2/M, which in turn impairs proper chromosome segregation and inflicts DNA damage on the daughter cells. Here we show that TopBP1 forms foci upon mitotic entry. In early mitosis, TopBP1 marks sites of and promotes unscheduled DNA synthesis. Moreover, TopBP1 is required for focus formation of the structure-selective nuclease and scaffold protein SLX4 in mitosis. Persistent TopBP1 foci transition into 53BP1 nuclear bodies (NBs) in G1 and precise temporal depletion of TopBP1 just before mitotic entry induced formation of 53BP1 NBs in the next cell cycle, showing that TopBP1 acts to reduce transmission of DNA damage to G1 daughter cells. Based on these results, we propose that TopBP1 maintains genome integrity in mitosis by controlling chromatin recruitment of SLX4 and by facilitating unscheduled DNA synthesis.

Introduction

Maintaining genome stability is of paramount importance for cell viability, and if compromised, may ultimately lead to development of cancer and other genetic diseases. The two key events that secure an intact copy of the genome for each daughter cell are (1) complete replication of the genome in S phase and (2) subsequent correct segregation of chromosomes in mitosis. The bulk of DNA replication is normally restricted to S phase, and ATR-dependent checkpoints support the completion of replication before entry into mitosis (Guo et al., 2000). Nevertheless, in response to replication stress, certain genomic regions termed common fragile sites (CFSs) have a propensity to remain under-replicated at the G2-to-M transition (Le Beau et al., 1998). Thus, under-replicated regions refer to DNA that is not fully replicated, but the molecular structures formed at these regions are unknown. Replication stress is a potential driver of the early steps of tumorigenesis (Bartkova et al., 2005; Halazonetis et al., 2008) and as a consequence >50% of recurrent deletions in cancers map to potential CFSs (Beroukhim et al., 2010; Bignell et al., 2010; Le Tallec et al., 2013). This underscores the importance of understanding cellular processing of under-replicated regions at the late stages of the cell cycle.

Sister chromatids must be disentangled before they can separate in anaphase. When sister chromatids are fully replicated, this reaction is performed by topoisomerase II–mediated decatenation, and most of the genome is decatenated before anaphase onset (Uhlmann et al., 2000; Oliveira et al., 2010). However, centromeric regions have a propensity to remain catenated in anaphase, giving rise to PICH-coated ultrafine anaphase bridges (UFBs) that are refractory to DAPI staining and are devoid of detectable histones (Baumann et al., 2007; Chan et al., 2007; Germann et al., 2014). During mitosis, under-replicated genomic regions can lead to the formation of various aberrant structures including replication stress–induced UFBs, which are distinguished from the centromeric UFBs by the presence of FANCD2 at the base of the bridge (Chan et al., 2009). In the following G1, under-replicated regions can nucleate 53BP1 nuclear bodies (53BP1 NBs) that protect the under-replicated DNA from untimely processing (Harrigan et al., 2011; Lukas et al., 2011). We have previously shown that TopBP1 colocalizes with PICH on a subset of UFBs (Germann et al., 2014). TopBP1 is a multifunctional protein involved in initiation of DNA replication, ATR-dependent checkpoint signaling, DNA repair, and transcriptional regulation (Mäkiniemi et al., 2001; Van Hatten et al., 2002; Yamane et al., 2003; Kumagai et al., 2006; Germann et al., 2011; Liu et al., 2013), but its exact role if any in mitosis is unclear.

Here we have investigated the role of TopBP1 during mitosis. Using endogenous fluorescent tagging in the avian cell line DT40, we have determined the choreography of TopBP1, PICH, 53BP1, FANCD2, and RPA. The fusion genes are under control of the endogenous promoter, allowing us to follow physiologically relevant concentrations of tagged proteins. We show that mitotic entry coincides with a dramatic increase in the number of TopBP1 foci, some of which persist

Correspondence to Vibe H. Oestergaard: vibe@bio.ku.dk; or Michael Lisby: mlisby@bio.ku.dk

Abbreviations used in this paper: APH, aphidicolin; araC, arabinofuranosyl cytidine; ATRi, ATR inhibitor; CFS, common fragile site; CPT, camptothecin; IAA, indole-3-acetic acid; UFB, ultrafine anaphase bridge; UFB-l, UFB-like.

The Rockefeller University Press $30.00
J. Cell Biol. Vol. 210 No. 4 565–582
www.jcb.org/cgi/doi/10.1083/jcb.201502107

throughout mitosis and transition into 53BP1 NBs in G1. We find that all RPA foci and most FANCD2 foci colocalize with mitotic TopBP1, and TopBP1 consistently localizes to replication stress–induced gaps and breaks on metaphase chromosomes, which is a common feature of CFSs. Importantly, we report two new functions of TopBP1 in mitosis. First, TopBP1 binds to under-replicated regions to support unscheduled DNA synthesis in mitosis. Second, TopBP1 is required for focus formation of the structure-selective nuclease SLX4, which promotes the resolution of recombinational repair intermediates (Fekairi et al., 2009; Muñoz et al., 2009; Svendsen et al., 2009). Consequently, precise temporal depletion of TopBP1 just before mitotic entry leads to a dramatic increase in 53BP1 NBs in G1 that may arise from combined defects in DNA synthesis at under-replicated regions and SLX4-mediated sister chromatid resolution.

Results

Entry into mitosis is accompanied by a burst in TopBP1 foci

During our previous study of TopBP1 localization in anaphase (Germann et al., 2014), we noticed that TopBP1 was present throughout mitosis. This prompted us to perform quantitative studies of TopBP1 localization during mitosis. First, we analyzed TopBP1 localization from 5 min before nuclear envelope breakdown (NEBD) until 5 min before anaphase onset. Using time-lapse microscopy, we analyzed a DT40 cell line expressing endogenous fluorescently tagged TopBP1. This showed that TopBP1 formed foci in mitosis at a frequency that increased 20-fold at NEBD and subsequently decreased 2.3-fold until anaphase onset (Fig. 1, A and B).

To get an indication of the underlying cause of the burst in TopBP1 foci at the onset of mitosis, we quantified TopBP1 foci in the absence or presence of aphidicolin (APH) and ICRF-193 (Fig. 1 A). Low concentrations of APH cause mild replication stress, allowing cells to enter mitosis with under-replicated DNA, whereas ICRF-193 inhibits decatenation by topoisomerase II. After exposure to APH for 20 h, TopBP1 foci were induced even before NEBD, and the frequency of TopBP1 foci was also mildly elevated at the subsequent time points in mitosis compared with the solvent-treated control. ICRF-193 exposure for 30 min before acquiring the time-lapse images also resulted in a mild induction of TopBP1 foci at the subsequent time points after NEBD.

To recapitulate our characterization of TopBP1 in a human cell line, we examined HeLa cells transiently expressing human GFP-TopBP1 and hH2B-mCherry. The quantification of TopBP1 foci in mitotic HeLa cells closely resembled that of DT40, showing that TopBP1 foci form at the onset of mitosis and decrease in number thereafter (Fig. 1, A and D). To rule out the possibility that the accumulation of TopBP1 foci at NEBD is due to its fluorescent tag, we performed immunofluorescence of endogenous TopBP1 in HeLa cells (Fig. 1 D). Quantification of immunostained TopBP1 foci again revealed a large number of foci at prometaphase, with the number of foci decreasing as cells progressed through mitosis (Fig. 1 E). Importantly, the immunostaining signal was completely abolished upon RNAi knockdown of TopBP1 (unpublished data).

During our studies of both human and chicken TopBP1 in mitosis, we also observed TopBP1 at the centrosomes (Reini et al., 2004), and TopBP1 foci with a thread-like appearance, which did not always overlap with chromatin marked by hH2B-mCherry (Fig. 1, B–D; and Fig. S1, A and B). For simplicity we refer to all TopBP1 structures colocalizing with hH2B-mCherry as foci.

In conclusion, mitotic entry coincides with a burst of TopBP1 foci of which approximately half disappear again during progression through mitosis. The frequency of TopBP1 foci is slightly induced by replication stress or topoisomerase II inhibition.

TopBP1 colocalizes with FANCD2 and RPA during mitosis

To investigate the nature of mitotic TopBP1 foci, we monitored the colocalization of TopBP1 and FANCD2 in preanaphase cells (prometaphase/metaphase). APH-induced replication stress induced an approximately twofold increase in both solitary FANCD2 foci and FANCD2 foci colocalizing with TopBP1 (Fig. 2, A and B). FANCD2 has been shown to form so-called sister foci at under-replicated regions including CFSs in mitosis (Chan et al., 2009; Naim and Rosselli, 2009). Similarly, we observed FANCD2 sister foci in mitosis (Fig. S1 C), and TopBP1 colocalized with approximately half of the FANCD2 foci but rarely with both of the FANCD2 sister foci. Specifically, for 71% of FANCD2 sister foci at least one of the sister foci was colocalizing with TopBP1 (35 out of 49).

To identify features of spontaneous and induced TopBP1 foci, we analyzed and quantified the localization of TopBP1 on metaphase macrochromosomes, with or without prior treatment with APH (Fig. 2, C and D). In response to APH, a 12-fold increase in the number of macrochromosomes with TopBP1 present at gaps/breaks was observed. Furthermore, TopBP1 localization at the chromosome ends is doubled in response to APH. Finally, we observed 5% of macrochromosomes with a TopBP1 focus at an internal site, and this category did not respond to APH. Thus, TopBP1 at internal sites and at chromosome ends are the main contributors of TopBP1 foci in unperturbed cells, whereas most of the APH-induced TopBP1 foci localize to gaps/breaks on metaphase chromosomes.

To obtain further insight into the DNA structures that are bound by TopBP1, we monitored colocalization of TopBP1 and the single strand binding protein RPA in preanaphase cells. RPA foci were only observed after treatment with APH or ICRF-193, but in these cases they virtually always colocalized with TopBP1 and FANCD2 (Fig. 2, E and F; and Fig. S1, D and E).

In conclusion, our data show that a subset of TopBP1 foci colocalizes with FANCD2 sister foci in mitosis and that TopBP1 binds to gaps and breaks on metaphase chromosomes, both of which are established hallmarks of replication stress at CFSs (Durkin and Glover, 2007; Chan et al., 2009).

The majority of TopBP1 foci remain on chromatin into anaphase

Our characterization of TopBP1 in early mitosis (Fig. 1) revealed that a fraction of mitotic TopBP1 foci persists after anaphase onset. To follow the fate of these TopBP1 foci, we set out to determine the frequency at which the persistent TopBP1 foci transition into the previously observed TopBP1-bound UFBs in anaphase (Germann et al., 2014). We therefore analyzed TopBP1 colocalization with PICH, a marker for UFBs (Baumann et al., 2007; Chan et al., 2007). Moreover, to address whether persistent TopBP1 foci tran-

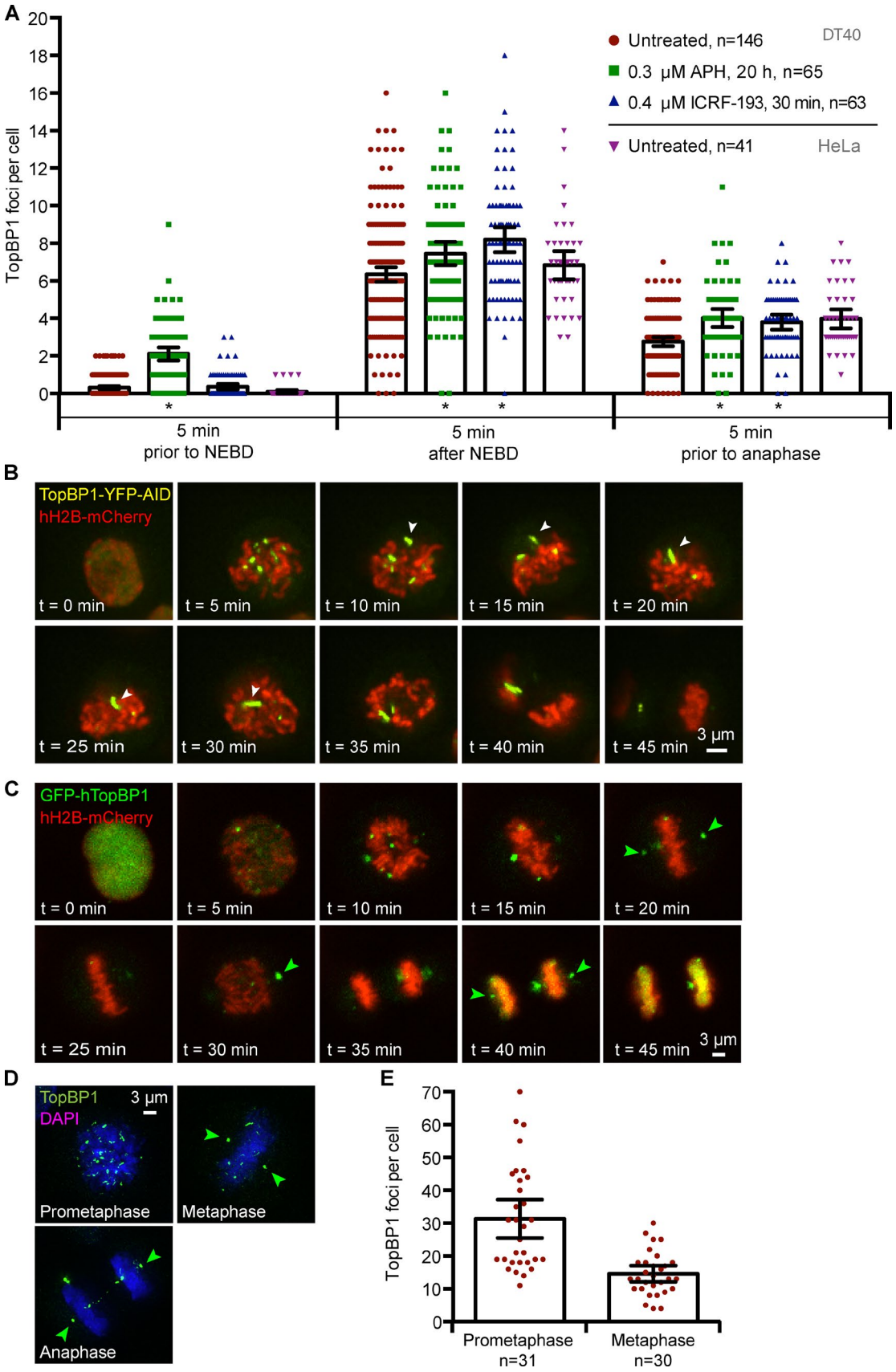

Figure 1. **TopBP1 foci accumulate upon NEBD and gradually disappear during progression of mitosis.** (A) Quantification of TopBP1 foci in mitosis in avian DT40 and human HeLa cells. The DT40 cell line RTP217 (TopBP1$^{YFP\text{-}AID/YFP\text{-}AID/YFP\text{-}AID}$/53BP1$^{TFP/WT}$/osTIR/hH2B-mCherry) and HeLa cells expressing GFP-hTopBP1 and hH2B-mCherry were imaged by time-lapse microscopy with a frequency of 5 min for 60 min. RTP217 was treated with 0.3 μM APH

sition into 53BP1 NBs in the following G1, we also fluorescently tagged 53BP1. Using this triple-tagged cell line, we performed time-lapse microscopy for 30 min starting at prometaphase (Fig. 3 A).

As previously described, we often observed TopBP1 foci in between the separating chromatin masses in anaphase (Germann et al., 2014). A fraction of these structures were PICH negative and never stretched out to fully bridge the sister chromatin masses. We therefore refer to such structures as UFB-likes (UFB-ls), because PICH is not present to verify the existence of a bona fide UFB. Furthermore, we observed PICH UFBs devoid of TopBP1 as well as chromatin-associated TopBP1 foci that did not localize to UFBs (Fig. 3 B). Consistent with our recent work (Germann et al., 2014), we found that the occurrence of TopBP1-bound PICH UFBs is much lower than TopBP1 UFB-ls (Fig. 3 C). Notably, the fraction of TopBP1-bound PICH UFBs is induced four- and twofold by APH and ICRF-193 treatment, respectively, whereas the frequency of noncolocalizing TopBP1 UFB-ls remained unchanged after APH treatment and decreased twofold in response to ICRF-193 treatment.

Our analysis also revealed that a large proportion of TopBP1 foci in anaphase and telophase are associated with the separating chromosome masses, distinguishing them from UFBs or UFB-ls. TopBP1 foci were induced in response to APH and ICRF-193 treatment. Surprisingly, a substantial fraction of PICH UFBs and TopBP1 foci contained 53BP1 already in mitosis, despite the recent findings that 53BP1 is actively excluded from chromatin in mitosis in human cells (Lee et al., 2014; Orthwein et al., 2014; Fig. 3 B). In contrast, 53BP1 rarely colocalized with TopBP1 UFB-ls (Fig. 3 C). The analysis showed that the various categories of TopBP1 UFBs and UFB-ls respond differently to replication stress or topoisomerase II inhibition and likely represent different molecular structures.

To further clarify whether TopBP1-bound UFBs result from replication stress, we performed time-lapse microscopy on the DT40 cell line expressing fluorescently tagged TopBP1, FANCD2, and PICH. In agreement with previous reports, we observed that FANCD2 associated with a subset of UFBs after APH treatment (Chan et al., 2009; Naim and Rosselli, 2009). Within this subset, FANCD2 localized either to the UFB termini and/or the central part of the UFB (Fig. 3 D). TopBP1 colocalized with FANCD2, either at the central part of the bridge or at one of the termini. The vast majority (98%) of TopBP1-bound UFBs were also associated with FANCD2 foci. In most instances, TopBP1 foci specifically colocalized with FANCD2 on the UFBs (90%; Fig. 3 E). Thus, TopBP1-bound UFBs correspond to the previously described FANCD2-associated UFBs, which are often linked to CFSs in human cells.

In summary, our results show that the majority of TopBP1 foci, which persist into anaphase in untreated cells, remain chromatin-associated (54%) and a substantial fraction become UFB-ls (42%), while only a small fraction localize to FANCD2-associated UFBs (4%).

Persistent TopBP1 foci transition into 53BP1 NBs

To follow the fate of the persistent TopBP1 foci from anaphase/telophase into G1, time-lapse microscopy was used. Complete chromatin decondensation was used as a criterion for entry into G1, and foci were quantified up to 10 min after decondensation. Most TopBP1 foci (>92%) in early G1 colocalized with 53BP1 NBs both with and without APH or ICRF-193 treatment, and both agents induced TopBP1 and 53BP1 colocalizing foci (1.5- and 2.2-fold, respectively). Consistently, TopBP1 was reported to colocalize with 53BP1 NBs in G1 in human cell lines (Cescutti et al., 2010; Lukas et al., 2011). APH or ICRF-193 treatment did not affect the fraction of 53BP1 NBs that did not colocalize with TopBP1, indicating that the fraction of 53BP1 NBs colocalizing with TopBP1 represented inherited DNA damage (Fig. 4 A).

Due to the profound spatial reorganization of the genome in the M-to-G1 transition, it is not always possible to track a specific focus. However, in a substantial number of time-lapse series, TopBP1 foci could be tracked from M into G1, allowing us to directly address which TopBP1 structures in mitosis transitioned into 53BP1 NBs in G1 (Fig. 4 B). The majority (82%) of the trackable TopBP1-associated 53BP1 NBs derived from chromatin-associated TopBP1 foci (Fig. 4 C). A small fraction of the trackable foci derived from UFBs (8%), or from the base of UFBs (10%), and the frequency of such events was increased by treatment with ICRF-193, APH, or the replication-blocking agent arabinofuranosyl cytidine (araC; Fig. S2). 53BP1 NBs were never observed to derive from UFB-ls or PICH-covered UFBs devoid of TopBP1.

Some UFBs were resolved early in anaphase and were therefore not trackable into G1. Assuming that such UFBs could turn into foci upon breakage or resolution, we predict that they would become TopBP1 foci facing the midzone. Thus we classified TopBP1 foci on separating chromosome masses into (1) centrosome facing (including foci in the central part of the chromosomes) or (2) midzone facing, and we determined the contribution of these two classes of TopBP1 foci to 53BP1 NBs in the following G1 (Fig. 4 D). The localization of TopBP1 foci that transition into 53BP1 NBs from the midzone region (43%) or from the centrosome facing region (57%) appeared largely random, suggesting that most 53BP1 NBs arise from TopBP1 foci that do not derive from UFBs.

In conclusion, persistent chromatin-associated TopBP1 foci frequently transition into 53BP1 NBs in the following G1, whereas UFB-ls and PICH-covered UFBs devoid of TopBP1 do not transition to 53BP1 NBs. Similar to TopBP1 foci, the TopBP1-bound UFBs also transition into 53BP1 NBs. However, due to their low abundance, their contribution is small. These data indicate that TopBP1 associates with a type of DNA structure that is likely to be transmitted as DNA damage to G1 daughter cells.

for 20 h, 0.4 µM ICRF-193 for 30 min, or 0.0125% DMSO (vol/vol, untreated) for 20 h before imaging. TopBP1 foci in each cell were scored 5 min before NEBD, 5 min after NEBD, and 5 min before anaphase. Asterisks indicate significant differences from the untreated ($P < 0.05$) and error bars represent 95% confidence intervals. The number of cells analyzed is indicated (*n*). (B) Representative time-lapse image sequence of a DMSO-treated RTP217 cell. White arrowheads indicate TopBP1 thread-like structure. (C) Representative time-lapse image sequence of an untreated HeLa cell expressing GFP-hTopBP1 and hH2B-mCherry. Green arrowheads indicate centrosome localization of TopBP1. (D) Representative images of HeLa cells immunostained for TopBP1. Green arrowheads indicate centrosome localization of TopBP1. (E) Quantification of TopBP1 structures in prometaphase and metaphase cells from the experiment described in D.

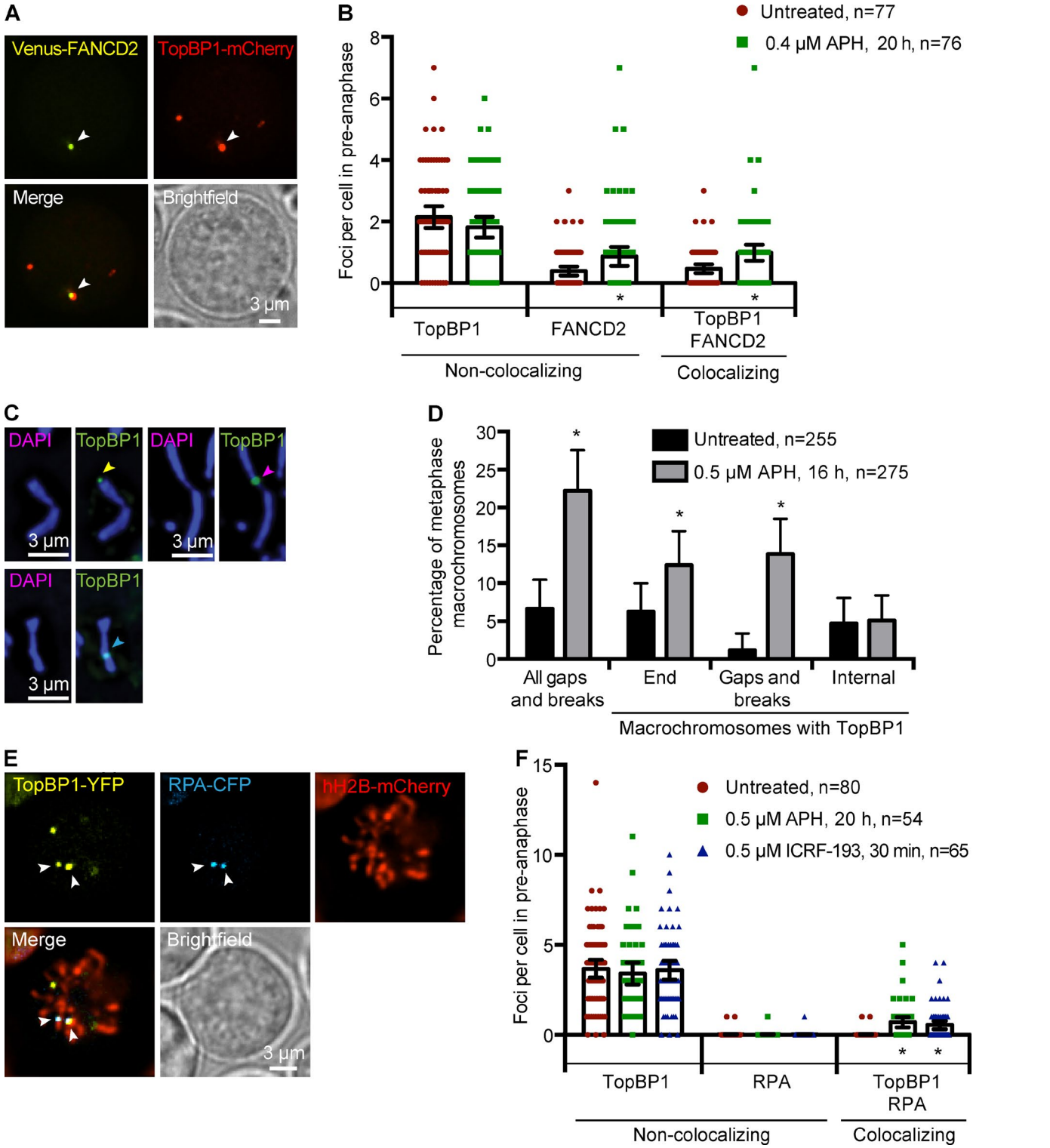

Figure 2. **TopBP1 colocalizes with FANCD2 in mitosis and binds to gaps and breaks on metaphase chromosomes.** (A) Representative images of the APH-treated DT40 cell line, RTP284 (PICH$^{TFP/WT}$/FANCD2$^{Venus/WT}$/TopBP1$^{mCherry/WT/WT}$). White arrowheads indicate colocalization of FANCD2 and TopBP1. (B) Quantification of FANCD2 and TopBP1 foci in live cell images. Images were captured 20 h after the addition of 0.4 µM APH or 0.0125% DMSO (vol/vol, untreated). TopBP1 and FANCD2 foci in preanaphase cells were quantified. (C) Representative images of TopBP1 localization on APH-treated metaphase macrochromosomes. Arrowheads indicate localization of TopBP1 foci on metaphase macrochromosomes at the end (yellow), a gap/break (green), or internal (pink). (D) Quantification of APH-induced gaps and breaks on metaphase macrochromosomes. Metaphase spreads with the DT40 cell line RTP164 (TopBP1$^{YFP\text{-}AID/YFP\text{-}AID/YFP\text{-}AID}$/osTIR) treated for 16 h with 0.5 µM APH or 0.0125% DMSO (vol/vol, untreated) before immunofluorescence staining against TopBP1-YFP-AID. All macrochromosomes were analyzed for gaps or breaks and TopBP1 foci localization. (E) Representative images of the APH-treated DT40 cell line RTP156 (TopBP1$^{YFP/WT/WT}$/RPA$^{CFP/WT}$/hH2B-mCherry). Arrowheads indicate colocalization of RPA and TopBP1. (F) Quantification of RPA and TopBP1 foci in live cell images. RTP156 cells were treated with 0.5 µM APH for 20 h, 0.5 µM ICRF-193 for 30 min, or 0.0125% DMSO (vol/vol, untreated) for 20 h before imaging. TopBP1 and RPA foci in preanaphase cells were quantified. For all graphs in this figure, asterisks indicate significant differences from the untreated ($P < 0.05$) and error bars represent 95% confidence intervals. The number of cells analyzed is indicated (*n*).

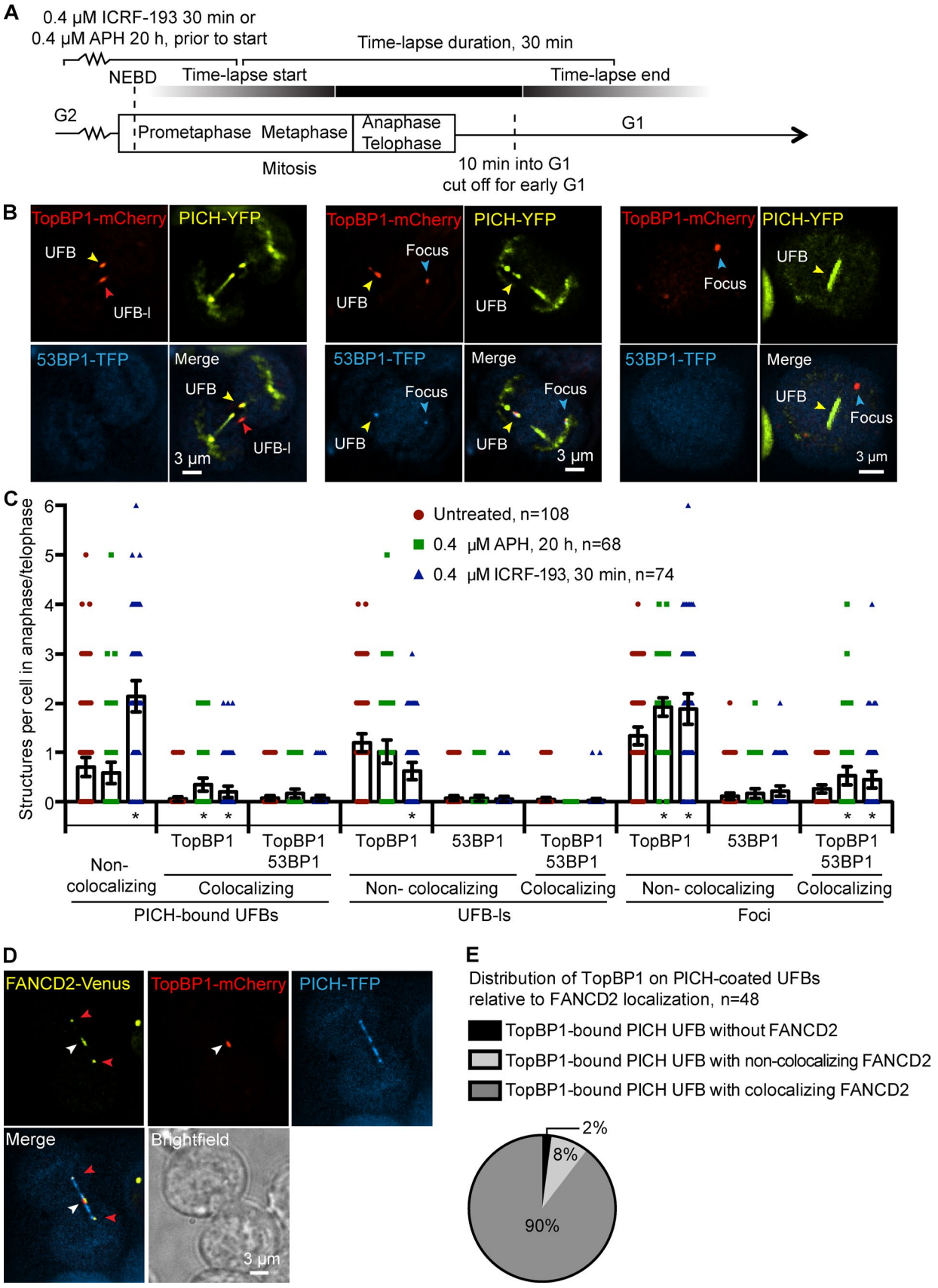

Figure 3. **TopBP1 binds several distinct structures in anaphase/telophase.** (A) Schematic representation of the experimental setup used in C, showing the duration of time-lapse microscopy and drug treatments relative to cell cycle phase. (B) Representative images of the DT40 cell line RTP252 (PICH$^{YFP/YFP}$/53BP1$^{TFP/WT}$/TopBP1$^{mCherry/WT/WT}$). (B, left) A DMSO-treated cell. The yellow arrowheads indicate the UFB bound by TopBP1 and the red arrowheads

TopBP1 colocalizes with sites of DNA synthesis in the G2/M phase

The gradual disappearance of TopBP1 foci during mitosis along with our finding that mitotic TopBP1 foci transition into 53BP1 NBs in G1 is indicative of ongoing DNA repair in mitosis. Moreover, our observation that TopBP1 foci are induced by APH and colocalize with FANCD2 suggests that a subset of TopBP1 foci in mitosis represents under-replicated DNA. Thus, we hypothesized that TopBP1 foci would colocalize with sites of DNA synthesis, similar to recent work showing that under-replicated regions including CFSs are sites of unscheduled DNA synthesis in mitosis or late G2 (Bergoglio et al., 2013; Bhat et al., 2013; Eykelenboom et al., 2013; Naim et al., 2013). To address whether TopBP1 foci localize to sites of unscheduled DNA synthesis, we pulsed cells with EdU for 20 min, followed by fluorescence labeling (Fig. 5, A and B). In a subset of mitotic cells, EdU incorporation was visible as distinct foci and this phenomenon was increased 13-fold after treatment with APH (Fig. 5, B and C), which is consistent with other studies (Bergoglio et al., 2013; Naim et al., 2013). More than 95% of EdU foci colocalize with TopBP1, whereas ∼20% of all TopBP1 foci colocalize with EdU in mitosis. As expected, APH-induced EdU incorporation was abolished by treatment with a high concentration of the replication inhibitor araC for 30 min before harvest (Fig. 5 C). TopBP1 foci were induced by araC treatment showing that the recruitment of TopBP1 to under-replicated regions does not depend on ongoing DNA synthesis. In agreement with our finding that TopBP1 and FANCD2 colocalize in mitosis (Fig. 2), we found that FANCD2 also localized to APH-induced EdU incorporation in mitosis (Fig. S3, A and B).

In conclusion, we find that a fraction of TopBP1 is present at sites of newly synthesized DNA in mitosis.

TopBP1 promotes replication stress–induced unscheduled DNA synthesis in G2/M

To investigate the requirement for TopBP1 at mitosis, we used the auxin-induced degradation system (Nishimura et al., 2009) to deplete endogenous TopBP1 as described previously (Germann et al., 2014), using the natural auxin, indole-3-acetic acid (IAA). To assess the efficiency of the IAA-mediated TopBP1 depletion, we directly measured levels of TopBP1-YFP-AID by fluorescence intensity (Fig. 6 A) and immunoblotting, as well as CHK1 phosphorylation after camptothecin (CPT) treatment (Fig. 6 B), the latter being dependent on TopBP1-mediated ATR activation (Kumagai et al., 2006). Combined, the results show that TopBP1-YFP-AID is ablated between 15 and 20 min after IAA addition. To evaluate the impact of TopBP1 depletion on mitotic progression in DT40 cells, we monitored the duration of mitotic phases with and without IAA-induced TopBP1 depletion for 30 min before NEBD. This analysis revealed no significant change in the timing of mitosis after TopBP1 depletion compared with untreated cells (Fig. 6 C).

Our observation that TopBP1 is recruited to under-replicated regions with ongoing DNA synthesis in late G2/M could suggest that TopBP1 promotes DNA synthesis at these sites. To test this, we pulsed APH-treated cells with EdU with or without IAA-induced TopBP1 depletion just before mitosis (Fig. 6 D). Depletion of TopBP1 resulted in a 1.7-fold reduction of APH-induced EdU incorporation in mitotic cells. The decrease in DNA synthesis could be complemented by ectopical expression of human TopBP1. To test if TopBP1 promotes DNA synthesis after NEBD, we disrupted the NLS of TopBP1 by deleting the last 17 amino acids of the C terminus (Bai et al., 2014). This TopBP1 version is almost exclusively cytoplasmic and only gains access to DNA upon NEBD, yet this version of TopBP1 completely reverts the drop in EdU incorporation caused by depletion of endogenous TopBP1 (Fig. 6, D and E). ATR, which is activated by TopBP1, has an important role in replication fork stabilization (Petermann and Helleday, 2010). To investigate whether TopBP1 supports replication through ATR activation, we treated EdU-pulsed cells with an ATR inhibitor (ATRi; Toledo et al., 2011). Inhibition of ATR per se did not reduce but rather increased APH-induced EdU incorporation, showing that TopBP1 promotes replication independently of ATR (Fig. 6 D). The applied concentration of ATRi completely inhibits CPT-induced CHK1 S345 phosphorylation, confirming that ATRi at the used concentration efficiently targets avian ATR (Fig. 6 F).

To address the effect of TopBP1 depletion at mitosis on formation of chromosome gaps/breaks, we quantified gaps/breaks on metaphase macrochromosomes. We find that TopBP1 depletion results in an increase in the formation of gaps/breaks, which is further increased by APH treatment (Fig. 6 G). Similar results have been found by siRNA depletion of human TopBP1 (Kim et al., 2005).

Based on these results, we conclude that TopBP1 stimulates unscheduled DNA synthesis at under-replicated regions in mitosis.

TopBP1 depletion in mitosis induces 53BP1 NBs

To test if TopBP1 is important for the repair of under-replicated regions in mitosis, we depleted TopBP1 in mitosis and quantified the 53BP1 NBs that arose in the following G1 within 10 min after chromatin decondensation (Fig. 7, A and B). Indeed, we found that TopBP1 depletion in mitosis increased the number of 53BP1 NBs per cell 2.9-fold. In fact, the effect on 53BP1 NB formation seen after depletion of TopBP1 is more severe than the effect of prolonged APH treatment, which resulted in a 1.5-fold increase in 53BP1 NBs per cell. To test whether 53BP1 NBs are affected by a lack of ATR activity, we also treated cells with ATRi during G2/M. To our surprise, ATRi suppressed the

indicate a TopBP1 UFB-l. (B, middle) An APH-treated cell. Yellow arrowheads indicate 53BP1 colocalization with TopBP1 on a PICH-coated UFB and blue arrowheads indicate a chromatin-associated TopBP1 focus. (B, right) A DMSO-treated cell. Yellow arrowheads indicate a UFB. Blue arrowheads indicate a chromatin-associated TopBP1 focus. (C) Quantification of TopBP1 and 53BP1 structures in mitosis. Cells were imaged by time-lapse microscopy with a frequency of 2 min for 30 min. Cells were monitored from anaphase through telophase and structures were scored in each cell. The maximum number of structures visible at one time point was noted as representative for the entire anaphase of a given cell. Cells were treated with 0.4 µM APH for 20 h, 0.4 µM ICRF-193 for 30 min, or 0.0125% DMSO (vol/vol, untreated) for 20 h before imaging. Asterisks indicate significant differences from the untreated ($P < 0.05$) and error bars represent 95% confidence intervals. The number of cells analyzed is indicated (*n*). (D) Representative live cell images of an APH-treated DT40 cell line RTP284 ($PICH^{TFP/WT}/FANCD2^{Venus/WT}/TopBP1^{mCherry/WT/WT}$). White arrowheads indicate colocalization between FANCD2 and TopBP1 on a PICH-coated UFB. Red arrowheads indicate FANCD2 sister foci at the terminus of a UFB. (E) Pie chart of the localization of FANCD2 foci relative to TopBP1-bound PICH UFBs after treatment with 0.3 µM APH for 20 h. The number of TopBP1-bound UFBs analyzed is indicated (*n*).

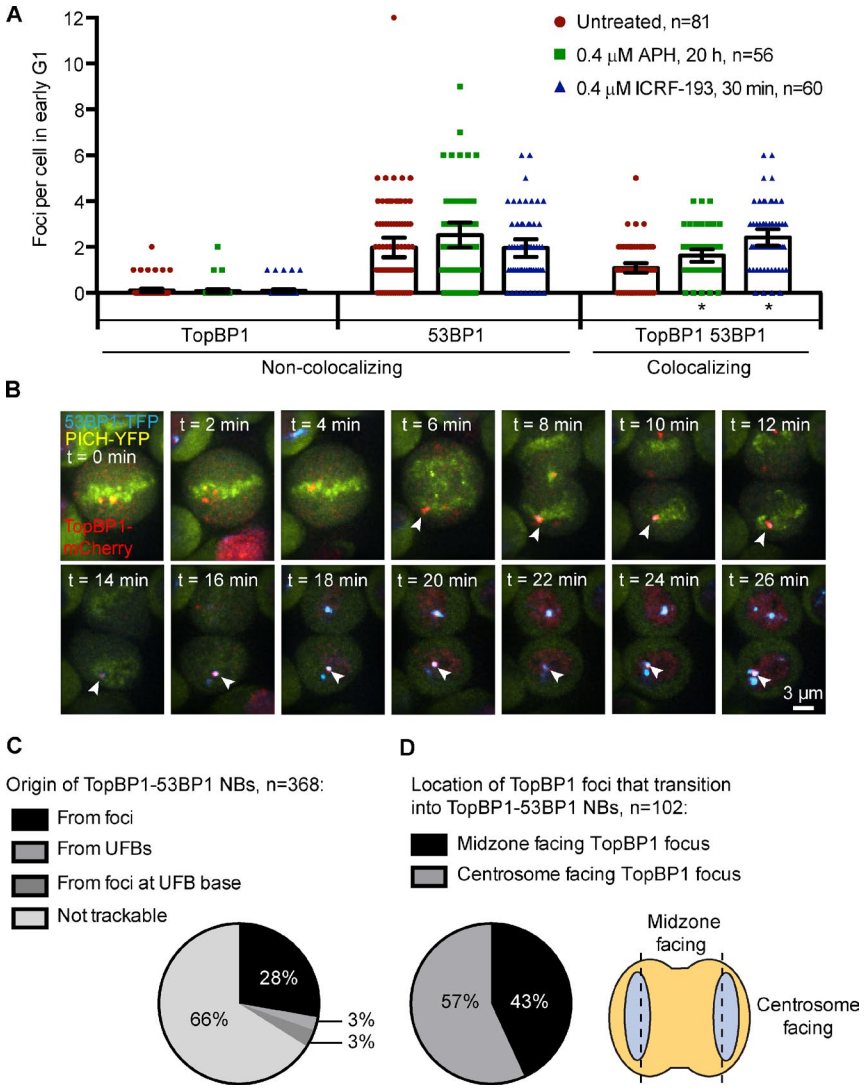

Figure 4. **Mitotic TopBP1 foci can transition into 53BP1 NBs in G1.** (A) Quantification of TopBP1 and 53BP1 structures in G1. Time-lapse microscopy of the DT40 cell line RTP252 (PICH$^{YFP/YFP}$/53BP1$^{TFP/WT}$/TopBP1$^{mCherry/WT/WT}$) with an imaging frequency of 2 min for 30 min. Cells were monitored from anaphase into early G1, which was defined as the first 10 min after chromatin decondensation. The maximum number of structures visible at one time point was noted as representative for the entire G1 of a given cell. Cells were treated with 0.4 μM APH for 20 h, 0.4 μM ICRF-193 for 30 min, or 0.0125% DMSO (vol/vol, untreated) for 20 h before imaging. Asterisks indicate significant differences from the untreated ($P < 0.05$) and error bars represent 95% confidence intervals. The number of cells analyzed is indicated (*n*). (B) Representative time-lapse image sequence of a DMSO-treated cell. Arrowheads mark a TopBP1 focus that turns into a 53BP1 NB in G1. (C) Pie chart of the anaphase/telophase TopBP1 structures that lead to 53BP1 NBs in G1. TopBP1 foci that colocalized with 53BP1 NBs were tracked as far back as possible from G1 into anaphase/telophase. The number of foci analyzed is indicated (*n*). (D) Pie chart showing the distribution on anaphase chromatin of the TopBP1 foci leading to 53BP1 NBs in G1. The number of foci analyzed is indicated (*n*). The schematic depicts the scoring of foci into the two categories: midzone or centrosome facing. Chromosome masses are indicated in blue.

formation of 53BP1 NBs. A more detailed analysis of 53BP1 NBs, where 53BP1 NBs were divided into two groups depending on signal intensity, termed weak NBs and strong NBs, showed that a combination of ATRi and TopBP1 depletion results in a threefold induction of weaker 53BP1 NBs, but a 1.8-fold decrease in strong 53BP1 NBs (Fig. 7 C). This result could indicate that ATRi inhibits an amplification step that can transform weak 53BP1 NBs into the strong 53BP1 NBs, but confirms that the functional role of TopBP1 in mitosis is independent of ATR kinase activity.

To determine the overall importance of TopBP1 for mitosis, we quantified the number of binucleated cells (Fig. 7 D) with or without TopBP1 depletion. TopBP1 depletion at mitosis caused a 2.3-fold increase in binucleated cells (Fig. 7 E), demonstrating that the fidelity of cell division is impaired in the absence of TopBP1.

In conclusion, we find that the absence of TopBP1 at mitosis leads to a higher frequency of DNA damage being transmitted to daughter cells.

TopBP1 is required for formation of SLX4 foci in mitosis

The observations that (1) only a subpopulation of TopBP1 colocalizes with EdU and (2) complete inhibition of unscheduled DNA synthesis induces fewer 53BP1 NBs than depletion of TopBP1 indicate that TopBP1 has an additional function apart from promoting unscheduled DNA synthesis. Hence, we hypothesized that mitotic TopBP1 is also required to disentangle late-replicating regions of the genome through recruitment of type II topoisomerases or resolvases. TopBP1 has been reported to interact with topoisomerase IIβ and SLX4, both of which could promote disentanglement of sister chromatids (Yamane et al., 1997; Gritenaite et al., 2014). First, we analyzed potential colocalization between TopBP1 and topoisomerase IIα and IIβ responsible for decatenation of fully replicated but catenated sister chromatids. Using endogenous fluorescence tagging of either topoisomerase IIα or IIβ, we were not able to detect any obvious colocalization with TopBP1 in mitosis (Fig. 8 A). We next addressed whether TopBP1 colocalizes with the resolvase scaffold protein SLX4 (Fekairi et al., 2009; Muñoz et al., 2009; Svendsen et al., 2009), which is involved in resolution of recombinational repair intermediates and possibly restart of stalled replication (Rouse, 2004). Chicken SLX4 holds an ubiquitin binding domain (UBZ), which is responsible for the interaction between FANCD2 and SLX4 (Yamamoto et al., 2011). To elucidate the dependency of FANCD2 on the potential colocalization between SLX4 and TopBP1, we included a SLX4 variant with

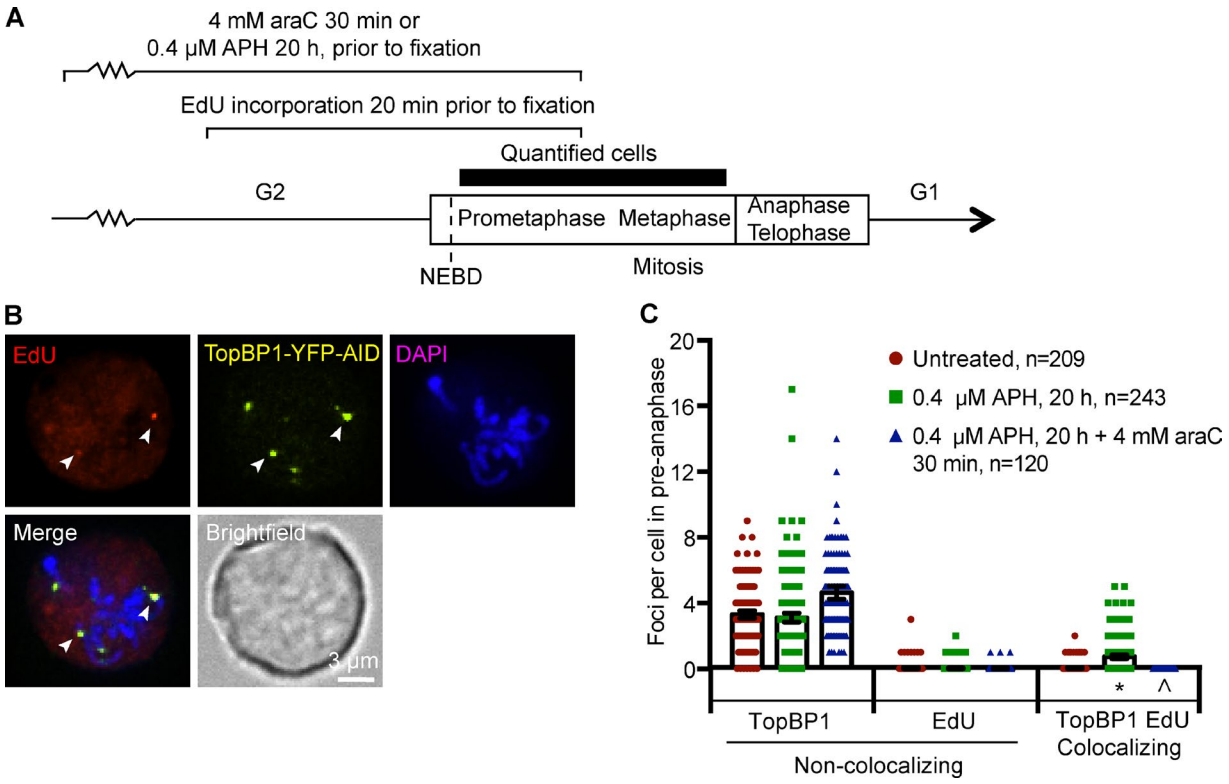

Figure 5. **TopBP1 colocalizes with DNA synthesis in mitosis.** (A) Schematic representation of the experimental setup used in B, showing the duration of drug and EdU treatments relative to cell cycle phase and time points for fixation. (B) Representative images of fixed DT40 cells RTP164 (TopBP1$^{YFP\text{-}AID/YFP\text{-}AID/YFP\text{-}AID}$/osTIR) treated with 0.4 μM APH for 20 h and pulse labeled with 20 μM EdU for 20 min. White arrowheads indicate TopBP1 foci colocalizing with EdU. (C) Quantification of EdU and TopBP1 foci in prometaphase and metaphase cells. Before imaging, cells were treated with 0.4 μM APH for 20 h, 0.0125% DMSO (vol/vol, untreated) for 20 h, or 0.4 μM APH for 20 h followed by 4 mM araC for 30 min. Before fixation, cells were pulse labeled with 20 μM EdU for 20 min. TopBP1 and EdU foci were quantified in prometaphase and metaphase identified based on chromatin condensation and alignment. Asterisks indicate significant differences from the untreated and the caret indicates significant differences from the APH-treated ($P < 0.05$). Error bars represent 95% confidence intervals. The number of cells analyzed is indicated (*n*).

the UBZ domain deleted. Chicken *SLX4-GFP* or *SLX4-UBZΔ-GFP* cDNA (Yamamoto et al., 2011) were stably transfected into a DT40 cell line expressing TopBP1-mCherry.

Consistent with previous studies, microscopy analyses of unperturbed anaphase cells revealed a high degree of colocalization between TopBP1 and SLX4 (Ohouo et al., 2010; Gritenaite et al., 2014). Specifically, 57% of all TopBP1 foci and 93% of all SLX4 foci colocalized (Fig. 8, A and B). Consistently, we also observed SLX4 colocalizing with TopBP1 foci and UFB-ls in anaphase as well as on PICH-covered UFBs (Fig. 8 D and Fig. S4). As shown in Fig. 1, there is a progressive reduction of TopBP1 foci through mitosis. The results shown in Fig. 8 B reveal that the frequency of colocalizing TopBP1-SLX4 foci declined more during mitosis than solitary TopBP1 foci. Thus, in preanaphase, TopBP1-SLX4 foci account for 57% of all TopBP1 foci, but this is reduced to 27% of all TopBP1 structures (foci, UFBs, and UFB-ls) in anaphase. SLX4-TopBP1 colocalizing structures in preanaphase and anaphase cells were induced 1.3- and 1.6-fold, respectively, by blocking replication with araC, thereby showing that SLX4 focus formation in mitosis does not depend on unscheduled DNA synthesis. Furthermore, the UBZ domain of SLX4 is not required for colocalization of TopBP1 and SLX4 in mitosis in DT40 cells. Consistently, FANCD2 was not required for SLX4 focus formation in mitosis (Fig. 8 C). To test whether TopBP1 is required for recruitment of SLX4, we analyzed SLX4 localization after TopBP1 depletion. Indeed, depletion of TopBP1 almost completely abolished SLX4 foci in mitosis (Fig. 8 E). In conclusion, TopBP1 is required for SLX4 focus formation in mitosis.

Discussion

Here we provide a detailed characterization of the localization of TopBP1 at mitosis (Fig. 9). We reveal that under unperturbed conditions as well as in response to replication stress, entry into mitosis is accompanied by a dramatic increase in chromatin-associated TopBP1 foci, both in HeLa and DT40 cells. In preanaphase cells, TopBP1 foci colocalize with FANCD2. In addition, TopBP1 binds to replication stress–induced gaps and breaks on metaphase chromosomes. Collectively, this shows that TopBP1 is recruited to replication stress-induced structures in mitosis. The majority of spontaneous TopBP1 foci localized at chromosome ends and at unbroken chromosomal sites. Future work is required to elucidate the nature of spontaneous mitotic TopBP1 foci. We also observed elongated thread-like TopBP1 structures of up to 3 μm adjacent to the condensed chromatin (Fig. S1). We speculate that these structures may represent recruitment of TopBP1 to loops of uncondensed damaged DNA or deposits of TopBP1 ejected from chromatin during chromosome condensation and/or repair.

During progression of mitosis, the number of TopBP1 foci gradually decreases. However, some TopBP1 foci (12%) persist through anaphase and telophase into G1, and the vast major-

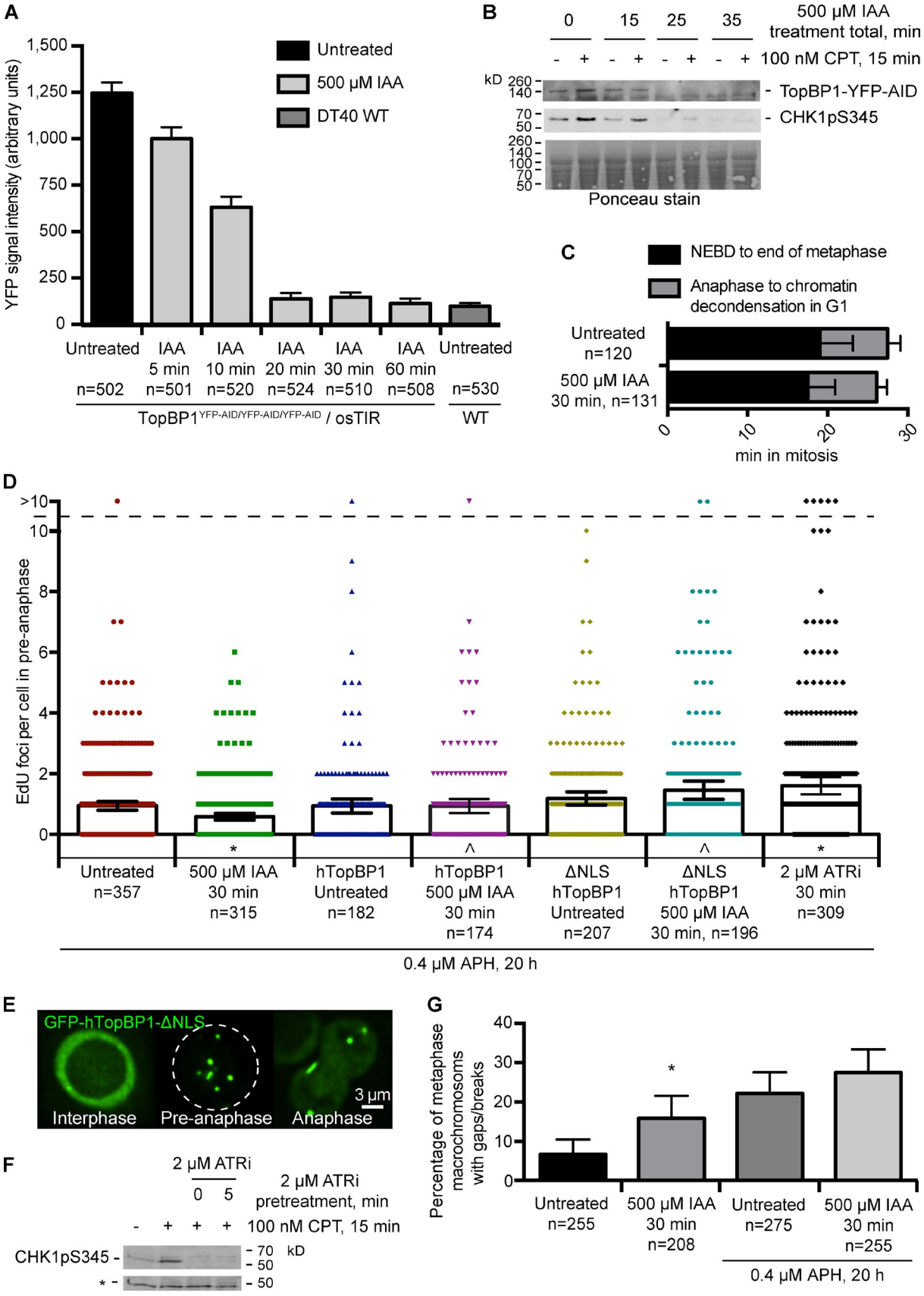

Figure 6. **Depletion of TopBP1 reduces EdU incorporation in mitotic cells.** (A) Quantification of TopBP1 depletion kinetics. Live cell imaging of the DT40 cell line RTP164 (TopBP1$^{YFP\text{-}AID/YFP\text{-}AID/YFP\text{-}AID}$/osTIR) and DT40 WT after addition of 500 μM IAA or 0.2% EtOH (vol/vol, untreated). The YFP intensity of cells was measured in Volocity and the average background was subtracted from all images. (B) Immunoblots of DT40 extracts to detect TopBP1-YFP-AID (top)

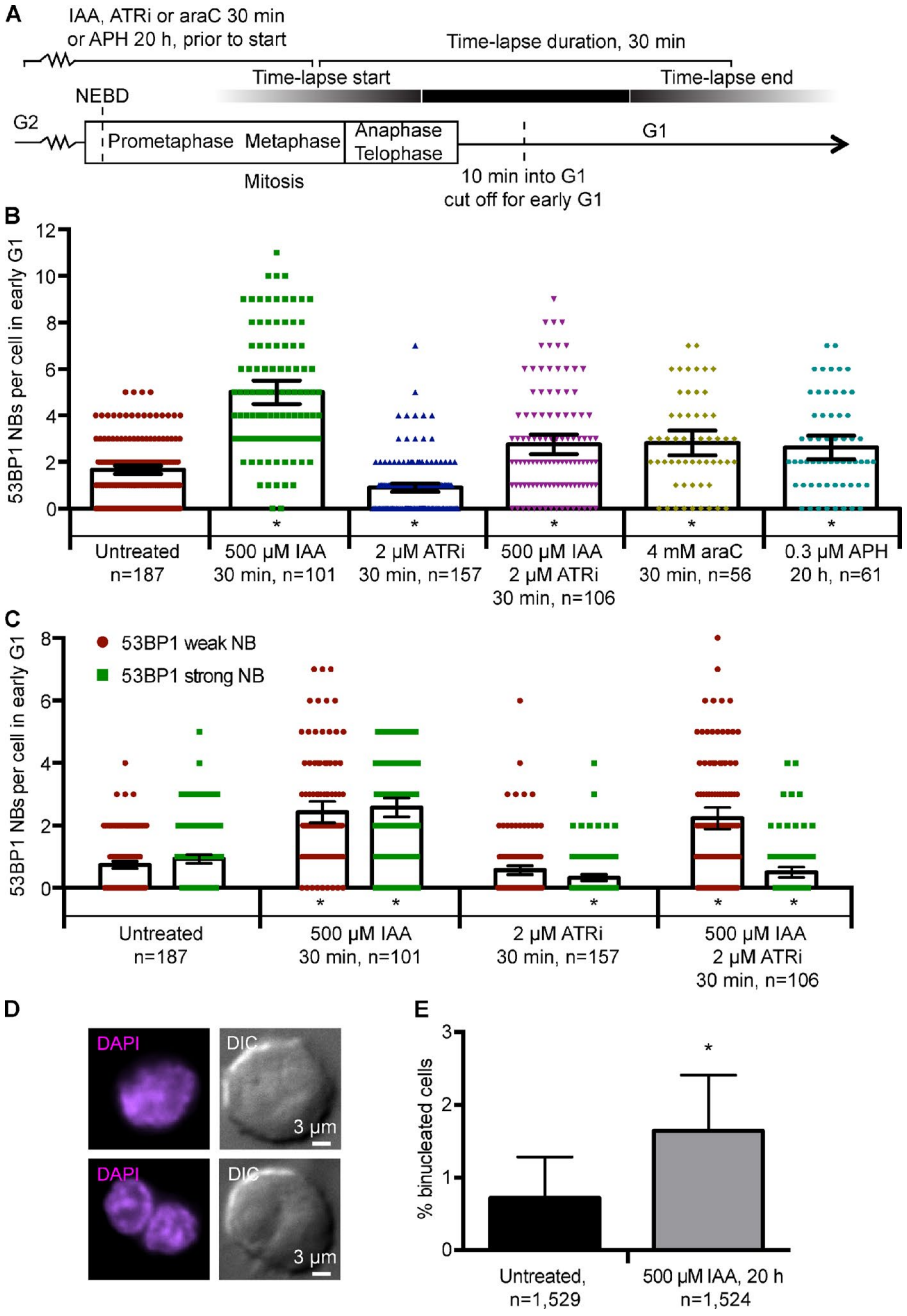

Figure 7. **Depletion of TopBP1 in mitosis induces 53BP1 NBs in the next G1.** (A) Schematic representation of the experimental setup, showing the duration of time-lapse microscopy and drug treatments relative to cell cycle phase. (B) Quantification of 53BP1 NBs in G1. Time-lapse microscopy of DT40 cells RTP217 (TopBP1$^{YFP\text{-}AID/YFP\text{-}AID/YFP\text{-}AID}$/53BP1$^{TFP/WT}$/osTIR/hH2B-mCherry) with an imaging frequency of 2 min for 30 min total. Cells were treated, alone or in combination, with 0.2% EtOH (vol/vol, untreated), 500 μM IAA, 2 μM ATRi, or 4 mM araC for 30 min or 0.3 μM APH for 20 h. Cells were monitored from anaphase to early G1, defined as the first 10 min after chromatin decondensation. The maximum number of structures visible at one time point was noted as representative for the entire G1 of a given cell. (C) Quantification of the fluorescence intensity of 53BP1 NBs in early G1. Images from the experiment in B were quantified in Volocity software. Strong NB denotes high-intensity structures and weak NB denotes low-intensity structures. (D) Representative images of a normal and a binucleated cell after treatment with 0.2% EtOH for 20 h. (E) Quantification of binucleated cells after TopBP1 depletion. The DT40 cell line RTP164 (TopBP1$^{YFP\text{-}AID/YFP\text{-}AID/YFP\text{-}AID}$/osTIR) was treated with 500 μM IAA or 0.2% EtOH (vol/vol, untreated) for 20 h and fixed. For all graphs in this figure, asterisks indicate significant differences from the untreated ($P < 0.05$) and error bars represent 95% confidence intervals. The number of cells analyzed is indicated (*n*).

or CHK1-pS345 (middle) in samples withdrawn at the indicated time points after exposure to 100 nM CPT and/or 500 μM IAA. CPT was added 15 min before harvest. Ponceau staining is shown as a control for equal loading (bottom). (C) Quantification of duration of mitosis in a DT40 cell. RTP217 (TopBP1$^{YFP\text{-}AID/YFP\text{-}AID/YFP\text{-}AID}$/53BP1$^{TFP/WT}$/osTIR/hH2B-mCherry) and RTP292 (hH2B-mCherry) were imaged by time-lapse microscopy with an imaging frequency of 1 min for 60 min after addition of 500 μM IAA or 0.2% EtOH (vol/vol, untreated) 30 min before NEBD. With hH2B-mCherry as a chromatin marker, time from NEBD to late metaphase, and from early anaphase to chromatin decondensation in G1 was recorded for each cell. (D) Quantification of EdU foci after TopBP1 depletion. DT40 cells RTP164 (TopBP1$^{YFP\text{-}AID/YFP\text{-}AID/YFP\text{-}AID}$/osTIR), RTP317 (TopBP1$^{YFP\text{-}AID/YFP\text{-}AID/YFP\text{-}AID}$/osTIR/human GFP-TopBP1), or RTP368 (TopBP1$^{YFP\text{-}AID/YFP\text{-}AID/YFP\text{-}AID}$/osTIR/human GFP-TopBP1-ΔNLS) were treated with 0.4 μM APH for 20 h. Next, the cells were treated with either 0.2% EtOH (vol/vol), 500 μM IAA, 4 mM araC, or 2 μM ATRi for 30 min and simultaneously pulse labeled with 20 μM EdU for the last 20 min before fixation and staining. EdU foci in prometaphase and metaphase cells were quantified. Asterisks indicate significant differences from the untreated ($P < 0.05$) and carets indicate significant differences between IAA-treated RTP164 and RTP317 or RTP368 ($P < 0.05$). (E) Representative live cell images of RTP368 at different cell cycle stages. (F) Immunoblot of DT40 extracts to detect CHK1-pS345. Where indicated, 100 nM CPT was added 15 min before harvest. 2 μM ATRi was added either concomitantly (0 min pretreatment) or 5 min before CPT as indicated. A cross-reacting band (asterisk) is shown as a loading control for the immunoblot. (G) Quantification of APH-induced or TopBP1 depletion–induced gaps and breaks on metaphase macrochromosomes. Metaphase spreads with the DT40 cell line RTP164 (TopBP1$^{YFP\text{-}AID/YFP\text{-}AID/YFP\text{-}AID}$/osTIR) treated for 16 h with 0.5 μM APH or 0.0125% DMSO (vol/vol, untreated) before a pulse with either 0.2% EtOH (vol/vol) or 500 μM IAA for 30 min and subsequent immunofluorescence staining against TopBP1-YFP-AID. Images were captured and all macrochromosomes were analyzed for gaps or breaks. Asterisks indicate significant differences from the untreated ($P < 0.05$). For graphs in this figure, error bars represent 95% confidence intervals in A, D, and F and standard deviation in C. The minimum number of cells analyzed is indicated (*n*).

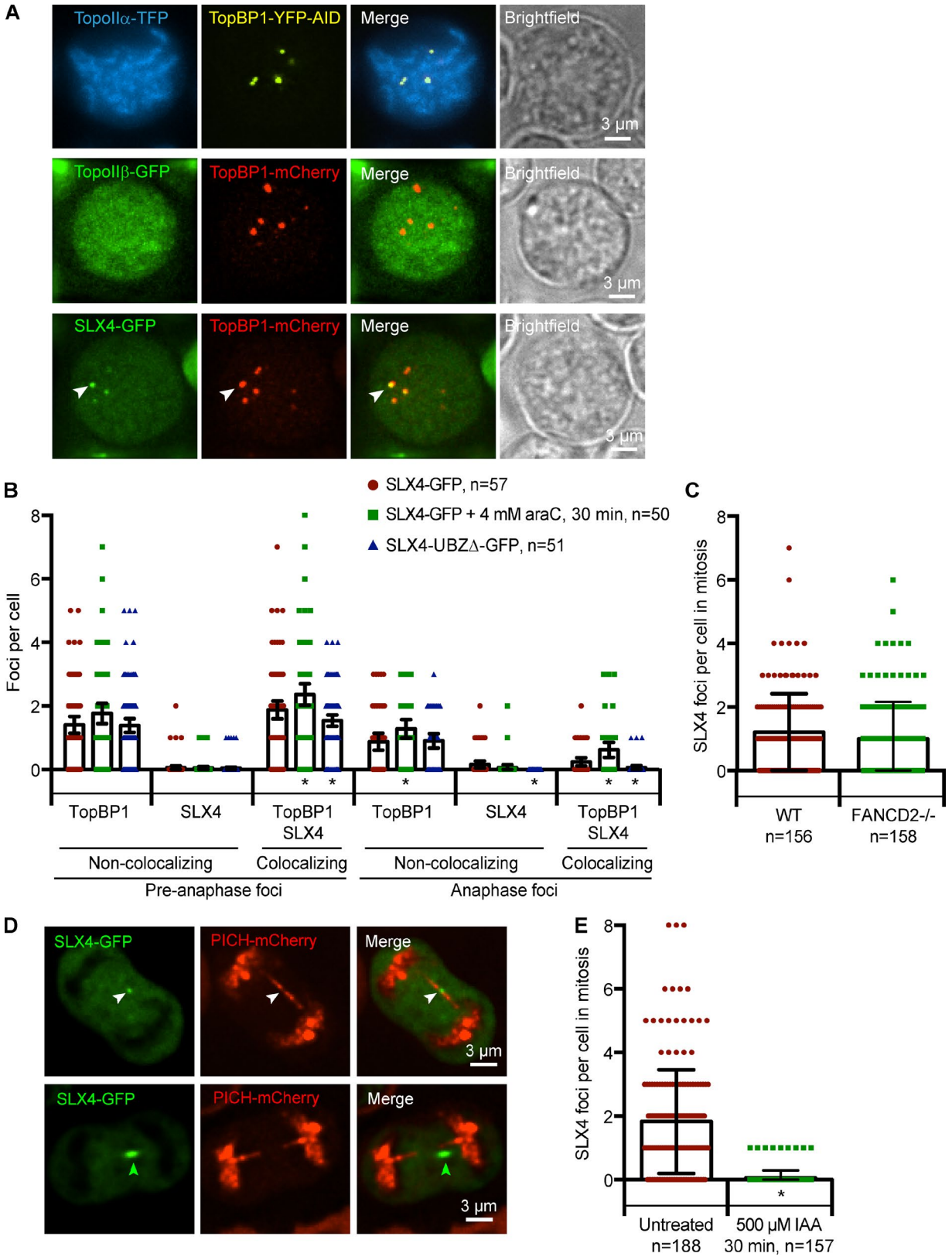

Figure 8. **TopBP1 colocalizes with SLX4 in mitosis.** (A) Representative images of TopBP1 in prometaphase cells with either Topo IIα, Topo IIβ, or SLX4. Localization of TopBP1 and Topo IIα, Topo IIβ, or SLX4 was examined from prometaphase to telophase in 40, 47, and 57 time-lapse videos, respectively. Images were selected from time-lapse microscopy experiments with the following cell lines: RTP315 (TopBP1$^{YFP\text{-}AID/YFP\text{-}AID/YFP\text{-}AID}$/Topo IIα$^{TFP/WT}$/osTIR), RTP328 (TopBP1$^{mCherry/WT}$/Topo IIβ$^{GFP/WT}$), or RTP302 (TopBP1$^{mCherry/WT}$/SLX4-GFP). RTP315, RTP328, and RTP302 were subjected to time-lapse microscopy with an imaging frequency of 2 min for 30 min. Arrowheads indicate a TopBP1 focus colocalizing with SLX4. (B) Quantification of SLX4 and TopBP1 structures in the cell lines RTP302 and RTP305 (TopBP1$^{mCherry/WT}$/SLX4-UBZΔ-GFP), using the experimental setup as shown in Fig. 3 A. Cells were incubated with or without 4 mM araC for 30 min before the start of the time-lapse experiments, and monitored from prometaphase to telophase. The maximum number of

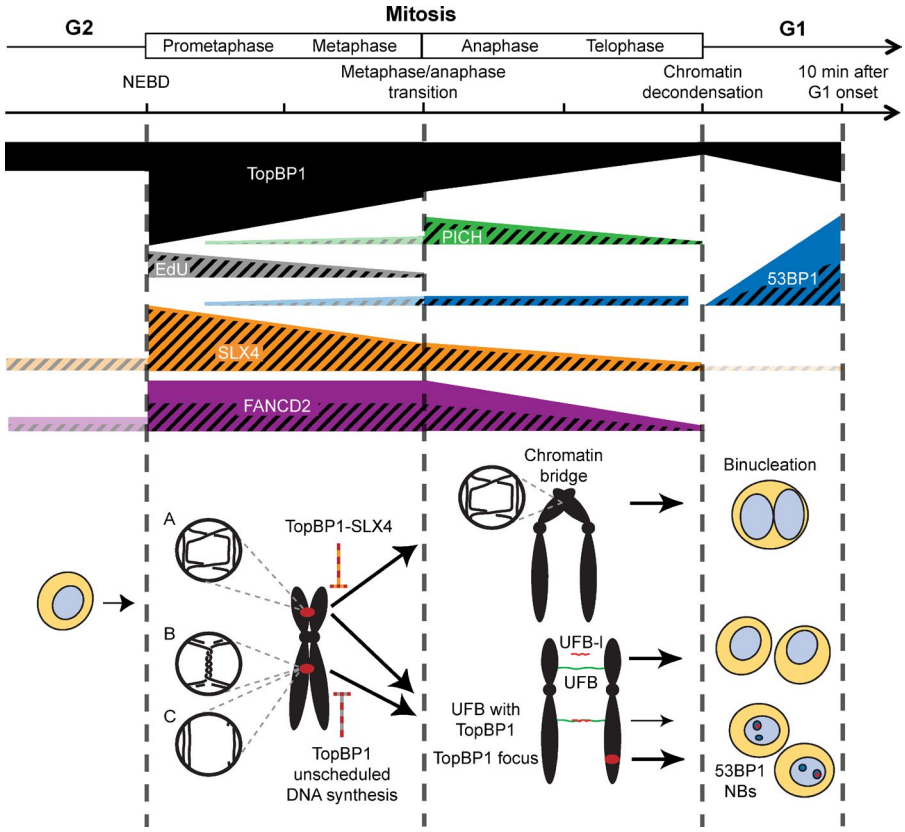

Figure 9. **Model for TopBP1 localization and function at mitosis.** (top) Overview of TopBP1 structures through mitosis based on our collective quantitative and qualitative data. Bar thicknesses are scaled to reflect the number of foci at a given time point where data were available. Hatched areas mark colocalization with TopBP1. (bottom) Hypothetical model for the functional role of TopBP1 in mitosis. In prometaphase, the sister chromatids remain interlinked by recombination intermediates (A) or unreplicated regions (B). Post-replicative gaps may also persist (C). TopBP1 (red ovals) may be recruited to these structures to facilitate their processing both by facilitating DNA synthesis to fill in unreplicated regions/post-replicative gaps as well as mediating resolution of Holliday junctions by SLX4. Resolution of Holliday junctions prevents formation of chromatin bridges, which may lead to mitotic catastrophe. If repair is not completed before anaphase, TopBP1 persists on DNA as chromatin-associated foci or TopBP1-bound UFBs (green/red thread). Both such structures can turn into 53BP1 NBs (blue ovals) in G1. TopBP1 is also observed on UFB-ls devoid of PICH (red thread). However, TopBP1 UFB-ls never transition into 53BP1 NBs. Likewise, PICH-covered UFBs devoid of TopBP1 (green thread) do not transition into 53BP1 NBs.

ity of these foci transition into 53BP1 NBs. The recruitment of 53BP1 to some TopBP1-bound structures in mitosis was surprising (Fig. 3 B) because of the recent reports that 53BP1 is actively excluded from chromatin in mitosis in human cells (Lee et al., 2014; Orthwein et al., 2014). Notably, the mitotic 53BP1 foci contain several orders of magnitude less 53BP1 than the prominent 53BP1 NBs in G1 estimated from the fluorescence intensity of 53BP1 foci. Hence, the ability to detect 53BP1 foci in mitosis may be a matter of fluorophore detection level. Alternatively, 53BP1 exclusion from mitotic chromatin is less efficient in chicken DT40 cells compared with human cells. Nevertheless, the frequency of 53BP1 structures in anaphase is significantly lower than that of TopBP1 structures (Fig. 3 C).

In anaphase, TopBP1 forms three distinct structures: UFBs, UFB-ls, and foci. The UFB-ls decrease in number in response to DNA damage–inducing drugs contrary to TopBP1 UFBs and foci. Thus UFB-ls most likely represent a distinct type of mitotic structure that does not share the same origin as foci or UFBs.

In line with the findings reported by Lukas et al. (2011), we find that the majority of UFBs do not give rise to 53BP1 NBs in G1. However, the TopBP1-bound UFBs transition into 53BP1 NB with a similar frequency to that of TopBP1 foci on chromatin, indicating that these TopBP1 structures are equally genotoxic. Yet the higher abundance of TopBP1 foci on chromatin compared with TopBP1-bound UFBs (ratio 7:1) accounts for the observation that the major source (92%) of inherited DNA damage visualized as 53BP1 NBs in G1 is chromatin-associated TopBP1 foci.

We speculate that the gradual disappearance of TopBP1 foci in prometaphase and metaphase reflects repair of under-replicated regions and/or resolution of repair intermediates. Supportive of this notion, we show that TopBP1 localizes to and promotes unscheduled DNA synthesis in mitosis. Furthermore, TopBP1 is responsible for recruitment of the structure-selective nuclease and scaffold protein SLX4 to chromatin in mitosis. These data suggest that TopBP1 acts as a last-minute savior to (1) promote DNA synthesis at under-replicated regions and to (2) direct SLX4-mediated resolution of persistent replication and DNA repair intermediates in mitosis. Consistently, depletion of TopBP1 around mitosis leads to an induction of 53BP1 NBs in the following G1, and the effect is more severe than complete inhibition of DNA replication in mitosis. Interestingly, two studies recently highlighted the critical role of SLX4's SUMO-dependent functions in the replication stress response including suppression of chromatin bridges and 53BP1 NBs (Guervilly et al., 2015; Ouyang et al., 2015).

The TopBP1-mediated stimulation of DNA synthesis could depend on the recruitment of SLX4 for homologous recombination–mediated restart of replication forks. Alter-

structures visible at one time point was noted as representative for preanaphase or anaphase of a given cell. (C) Quantification of SLX4 foci in live cell images of the DT40 cell line RTP302 and RTP349 (SLX4-GFP/FANCD2$^{-/-}$). SLX4 structures in mitotic cells were quantified. (D) Representative images of a PICH-coated UFB bound by SLX4 and a SLX4-bound UFB-l. Images were captured with the following cell line: RTP335 (PICH$^{mCherry/mCherry}$/SLX4-GFP). White arrowheads indicate a UFB bound by SLX4. Green arrowheads indicate an SLX4 UFB-l. (E) Quantification of SLX4 foci in live cell images of the DT40 cell line RTP319 (TopBP1$^{YFP\text{-}AID/YFP\text{-}AID/YFP\text{-}AID}$/SLX4-GFP/osTIR). Images were captured 30 min after addition of 500 µM IAA. SLX4 structures in mitotic cells were quantified. For all graphs in this figure, asterisks indicate significant differences from the untreated ($P < 0.05$) and error bars represent 95% confidence intervals. The number of cells analyzed is indicated (*n*).

natively, TopBP1 recruits polymerases or replication fork remodelers to promote unscheduled DNA synthesis (Mäkiniemi et al., 2001; Wang et al., 2013). The exact mechanisms by which TopBP1 facilitates DNA synthesis in mitosis will be subject to future studies.

Only a small fraction of TopBP1 foci colocalized with EdU incorporation, which may reflect that not all TopBP1-bound DNA damage requires DNA synthesis for repair or could be due to the detection limit of our assay. To test the latter hypothesis, we determined if prolonged EdU pulsing would increase the percentage of TopBP1 foci colocalizing with EdU. A longer pulse did increase the fraction of TopBP1 colocalizing with EdU; however, it also elevated the fraction of EdU foci without TopBP1 (Fig. S5).

Several recent publications have reported that Holliday junction resolution/dissolution is subject to a temporal control with the BLM-dependent dissolution pathway acting in S/G2, whereas resolution by SLX4/MUS81 is favored in G2/M and GEN1-mediated resolution acts later in mitosis (Matos et al., 2011, 2013; Gallo-Fernández et al., 2012; Szakal and Branzei, 2013; Wyatt et al., 2013; Brandao et al., 2014; Gritenaite et al., 2014). Our observations of TopBP1 and SLX4 colocalization throughout mitosis together with the finding that SLX4 focus formation in mitosis is dependent on TopBP1, uncovers TopBP1 as a potential spatio-temporal regulator of Holliday junction resolvase activity.

The TopBP1-dependent formation of SLX4 foci in mitosis reported here also offers new insight to our understanding of the involvement of TopBP1 and its yeast homologue Dpb11 in suppression of chromatin bridges in anaphase (Germann et al., 2014). In both yeast and vertebrate cells, depletion of Dpb11/TopBP1 greatly induces the formation of chromatin bridges, and detailed analyses in yeast revealed that chromatin bridge formation largely depends on homologous recombination. The TopBP1-dependent formation of SLX4 foci in mitosis suggests that TopBP1 suppresses chromatin bridges by promoting resolution of homologous recombination intermediates before anaphase.

Surprisingly, we find that both TopBP1 foci in mitosis as well as 53BP1 NBs in G1 are induced by treatment with the topoisomerase II inhibitor ICRF-193. This suggests that 53BP1 NBs in G1 do not just derive from under-replicated regions. Rather, perturbations in chromatin condensation may also cause DNA damage (Samejima et al., 2012). However, the interpretation of the ICRF-193–induced effects is complicated by the fact that ICRF-193 is not merely blocking the catalytic cycle of topoisomerase II, but also traps topoisomerase II clamped onto DNA (Roca et al., 1994), which actively poisons cells (Oestergaard et al., 2004) and perturbs chromatin structure (Germe and Hyrien, 2005).

In summary, we show that in mitosis TopBP1 functions to avoid transmission of DNA damage to daughter cells by promoting proper localization of the SLX4 resolvase and by facilitating DNA synthesis. This notion is supported by the observation that depletion of TopBP1 at mitosis results in a dramatic increase in 53BP1 NBs in the following G1.

Materials and methods

All DT40 cell lines, plasmids, and primers used in this study are listed in Tables S1, S2, and S3, respectively. All experiments were performed in triplicate. The *FANCD2*$^{-/-}$ cell line and plasmids for generating *SLX4-GFP* and *SLX4-UBZΔ-GFP* cell lines were a gift from S. Takeda (Kyoto University, Kyoto, Japan). The plasmids for generating the *TopoIIα-FLAG* and *TopoIIβ-GFP* cell lines were a gift from C.J. Farr (University of Cambridge, Cambridge, England, UK). The ATR inhibitor was a gift from J. Lukas and L.I. Toledo (The Novo Nordisk Foundation Center for Protein Research, University of Copenhagen, Copenhagen, Denmark).

DT40 cell culture

DT40 cells were cultured in RPMI 1640 medium GlutaMAX (Gibco) supplemented with 2% chicken serum (Gibco), 8% FBS (Gibco), 2 mM L-glutamine (Gibco), 55 µM β-mercaptoethanol, 50 U/ml penicillin, and 50 µg/ml streptomycin at 39°C with 5% CO_2.

HeLa cell culturing, live cell microscopy, and immunofluorescence microscopy

HeLa cells were maintained in DMEM with 10% fetal calf serum for 48 h before live cell analysis. HeLa cells were cotransfected with DNA vectors encoding GFP-TopBP1 and hH2B-mCherry. For efficient TopBP1 depletion, cells were subjected to a double knockdown protocol using 10 nM of TopBP1 siRNA oligo (Ambion Silencer Select, s21825) with transfection on days one and two. As a control, 50 nM of Luciferase siRNA oligo (VC300B2; Sigma-Aldrich) was used. Cells were fixed on day three and stored in PBS for later analysis by immunofluorescense microscopy. Live cell microscopy was performed as described previously using a microscope (Deltavision Elite; GE Healthcare) equipped with a 40× oil objective lens with a numerical aperture of 1.35 (GE Healthcare; Kruse et al., 2013). During live cell microscopy, cells were maintained at 37°C in Leibovitz's L-15 medium (Gibco) containing 10% fetal calf serum. SoftWoRx software (GE Healthcare) was used to acquire and subsequently analyze the data. For immunofluorescence microscopy, HeLa cells were grown as an asynchronous culture on coverslips and washed once with PBS before fixing with 100% methanol for 20 min at −20°C. Cells were blocked in 10% FBS in PBS for 30 min before incubation with the polyclonal rabbit anti-TopBP1 antibody (A300-111A, 1:200; Bethyl Laboratories, Inc.) in 0.1% FBS in PBS for 1 h at room temperature. Unbound primary antibodies were removed by washing four times for 5 min in PBS at room temperature followed by incubation with secondary antibodies (Alexa Fluor 488; 1:1,000; Invitrogen) for 45 min. Coverslips were then washed four times for 5 min in PBS before mounting with Vectashield mounting medium containing DAPI. Z stacks 200 nm apart were recorded on a microscope (DeltaVision Elite) using a 100× oil objective lens (numerical aperture 1.40) followed by deconvolution using SoftWoRx. The DeltaVision Elite microscope was equipped with a CoolSNAP HQ2 camera (Photometrics).

Generation of DT40 knock-in and random integration constructs

In this study, DT40 genes were endogenously tagged at their 3′ termini. The 53BP1-TFP, TopBP1-mCherry, and TopoIIα-TFP knock-in constructs were subcloned from the published constructs pRTP7, pVHO3, and pX33 (Johnson et al., 2009; Germann et al., 2011; Oestergaard et al., 2012). Constructs for random integration of osTIR and SLX4-GFP were subcloned from the published constructs pNHK65 (Nishimura et al., 2009) and pX45 (Yamamoto et al., 2011). The mCherry tags were amplified from pmCherry-C1 using the primer pairs VO128/VO129 and RTP59/RTP60 for TopBP1 and PICH tagging, respectively. The primer pairs were designed to facilitate directional cloning. The hTopBP1-ΔNLS mutant was created by PCR using pEGFP-C1-hTopBP1 and the primer pairs RTP68/RTP72, introducing a stop codon

deleting the last 17 amino acids. The amplified PCR products were cloned into the pCR2.1-TOPO vector (Invitrogen) and the coding region was sequenced (Eurofins MWG Operon).

For assembly of osTIR transgene construct (pRTP24), osTIR was subcloned from pNHK65 into pExpress using the restriction sites BamHI–Eco47III and Eco32I–BglII, respectively. pExpress-osTIR was sequentially cut with the restriction enzymes OliI and KpnI. pLOX-NEO was sequentially treated with the enzymes SalI, mung bean nuclease, and KpnI. Subsequently, the NEO resistance cassette was subcloned into pExpress-osTIR.

For assembly of the TopBP1-mCherry knock-in construct (pRTP27), the mCherry tag was subcloned into a version of pVHO3 before the insertion of the BamHI flanked resistance cassette, using restriction sites XbaI–BglII. Subsequently, a BSR resistance cassette was subcloned from pLOX-BSR into the knock-in construct using restriction sites BamHI and BglII, respectively.

For assembly of the PICH-mCherry knock-in constructs (pRTP32 and pRTP33), the mCherry tag was subcloned into pRTP17 using restriction sites EcoRI–SalI, creating pRTP32. Subsequently, to create pRTP33, a PAC resistance cassette was subcloned from pRTP9 into pRTP32 using restriction site EcoRI–KspAI.

For assembly of a GFP-hTopBP1-ΔNLS transgene construct under expression control of chicken β-actin promoter (pRTP46), GFP-hTopBP1-ΔNLS was subcloned into pExpress using the restriction site NheI. Subsequently, a PURO resistance cassette was subcloned from pLOX-PURO into pExpress-GFP-hTopBP1-ΔNLS using the restriction sites PvuII and SmaI, respectively.

For assembly of the 53BP1-TFP knock-in construct (pRTP31), the TFP tag was subcloned from pRTP17 into pRTP7 using restriction sites SalI–SmaI.

For assembly of the TopoIIα-TFP knock-in construct (pRTP37), the TFP tag was subcloned from pRTP31 into pX33 using restriction sites SalI–BamHI. Subsequently, a PAC resistance cassette was subcloned from pLOX-PURO into the knock-in construct using restriction site BamHI.

For assembly of SLX4-GFP under expression control of chicken β-actin promoter (pRTP40), SLX4-GFP was subcloned from pX45 into pExpress using the restriction sites NheI–AanI and NheI–Eco32I, respectively. Subsequently, a BSR resistance cassette was subcloned from pLOX-BSR into pExpress-SLX4-GFP using restriction sites PvuII and SmaI, respectively.

For assembly of GFP-hTopBP1 transgene construct under expression control of chicken β-actin promoter (pRTP38), GFP-hTopBP1 was subcloned from pEGFP-C1-hTopBP1 into pExpress using the restriction sites NheI–KspAI and NheI–Eco32I, respectively. Subsequently, a BSR resistance cassette was subcloned from pLOX-BSR into pExpress-GFP-hTopBP1 using the restriction site BamHI. The plasmid pEGFP-C1-hTopBP1 was provided by C.S. Sorensen (Biotech Research and Innovation Center, University of Copenhagen, Copenhagen, Denmark).

The construct for GS tagging of endogenous FANCD2 was made by amplifying the 3′ arm using the SpeI-adapted forward primer VO300 and the NotI-adapted reverse primer VO301. The 3′ arm was cloned into pBlueScript as a SpeI–NotI fragment. A sequence encoding an N-terminal Venus tag was made by adapting a Venus-encoding sequence with a 5′ BamHI site using the primer VO67 and a 3′ SpeI site using the primer VO252, which was then inserted as a BamHI–SpeI fragment. A 5′ arm was generated using the SalI-adapted forward primer VO302 and a BamHI-adapted reverse primer VO303. This fragment was inserted as a SalI–BamHI fragment. Finally, the PAC resistance cassette was inserted as a BamHI fragment.

Generation of tagged DT40 cell lines

The targeting constructs were linearized with NotI and transfected into DT40 cells by electroporation (gene pulser Xcell; Bio-Rad Laboratories). Transfectants harboring the PAC, NEO, and BSR resistance genes were selected in the presence of 0.5 µg/ml puromycin, 2 mg/ml G418, and 20 µg/ml blasticidin, respectively. The resistance cassettes were loxed as described previously (Arakawa et al., 2001). In brief, cell lines were transiently transfected with cDNA encoding the Cre recombinase and subsequently dilution cloned to obtain single colonies. Loss of selection markers was tested by treating the resulting cell lines with puromycin, G418, or blasticidin.

DT40 live cell and immunofluorescence microscopy

For live cell microscopy, exponentially growing DT40 cells were imaged at 39°C in growth medium, and mounted on µ-slides 30 min before imaging (Ibidi). Where indicated in the figures, the following drugs were added for the indicated time before imaging: 500 µM IAA (Sigma-Aldrich), 2 µM ATRi (Toledo et al., 2011), 0.4 µM APH (Sigma-Aldrich), 0.3 µM APH, 0.4 µM ICRF-193 (Sigma-Aldrich), 4 mM cytosine β-D-arabinofuranoside (araC; C1768; Sigma-Aldrich), 0.2% EtOH (vol/vol), or 0.0125% DMSO (vol/vol). Immunofluorescence microscopy of DT40 cells and metaphase spreads were performed at room temperature.

Fluorophores were visualized on a wide-field microscope (AxioImager Z1; Carl Zeiss) equipped with a 100× objective lens (Plan Apochromat, NA 1.4; Carl Zeiss), a cooled charge-coupled device (CCD) camera (Orca-ER; Hamamatsu Photonics), differential interference contrast (DIC), and an illumination source (HXP120C; Carl Zeiss); or on a wide-field microscope (DeltaVision Elite; Applied Precision) equipped with a 100× objective lens (U-PLAN S-APO, NA 1.4; Olympus), a cooled EM CCD camera (Evolve 512; Photometrics), and a solid-state illumination source (Insight; Applied Precision). Images were acquired using Volocity (PerkinElmer) or softWoRx (Applied Precision) software. Images were processed and quantitative measurements of fluorescence intensities were performed with Volocity software (PerkinElmer). Images were pseudocolored according to the approximate emission wavelength of the fluorophores. Fluorescent proteins used in DT40 were TFP (pmTurquoise2-N1; Goedhart et al., 2010), CFP (enhanced CFP; Takara Bio Inc.), YFP (enhanced YFP; Takara Bio Inc.), Venus (Nagai et al., 2002), GFP (enhanced GFP; Cormack et al., 1996), and mCherry (Shaner et al., 2004).

Centrosome-like TopBP1 foci were excluded from all quantifications made in this study. Representative pictures presented in figures were deconvoluted and gamma adjusted using Volocity software.

Metaphase spreads

Cells were grown for 16 h with 0.5 µM APH and treated with 0.1 µg/ml Colcemid (Life Technologies) for 150 min before harvest. Next, cells were swelled in hypotonic buffer (20% FBS [vol/vol], 15 mM KCl) for 15 min before centrifugation at 1,000 rpm onto cytospin slides (Thermo Fisher Scientific). Cells and metaphase spreads were fixed on the slide with 3% paraformaldehyde (Sigma-Aldrich) for 10 min. Subsequently, the slide was immersed in KCM buffer (120 mM KCl, 20 mM NaCl, 10 mM Tris/HCl, pH 8.0, 0.5 mM EDTA, and 0.1% Triton X-100) for 10 min and then washed with PBS (10 mM phosphate and 154 mM NaCl, pH 7.4). The slides were then drained and fixed metaphase spreads were incubated with blocking solution (PBS-T with 3% BSA) for 20 min followed by incubation with GFP antibody (1:1,000; Roche) for 25 min at 37°C. Next, slides were washed twice in PBS-T (PBS with 0.1% Tween 20) and drained before incubation in secondary Alexa Fluor 488–conjugated anti–mouse IgG (1:1,000; catalogue no. A21121; Invitrogen). Finally, slides were washed twice in

PBS-T, drained, and mounted with DAPI-containing mounting buffer (85% glycerol, 2.5% n-propyl-gallate with 1.5 µg/ml DAPI).

Time-lapse microscopy in mitosis and G1

Unless otherwise stated, DT40 cells were imaged by time-lapse microscopy with an imaging frequency of 2 min for 30 min total. Cells were monitored from anaphase through telophase into G1 and structures were scored in each cell. The maximum number of structures visible at one time point was noted as representative for the entire preanaphase, anaphase/telophase, or G1 of a given cell. Chromatin condensation and decondensation, visualized by hH2B, was used to define the boundary between G2 and mitosis, and between anaphase/telophase and G1, respectively. G1 cells were only counted if they could be tracked from mitosis into G1 for a minimum of three time points and followed for a maximum of five time points. TopBP1 foci in G1 were tracked back into mitosis as far back as possible, and the originating structure was noted. Furthermore, the localization of the structures relative to anaphase chromatin was noted.

Replication assay

For EdU incorporation, cells were treated with 20 µM EdU for 20 min before cell harvest. Cells were washed and resuspended in PBS, and allowed to adhere to poly-L-lysine–coated coverslips for 10 min. Cell fixation, permeabilization, and EdU detection were performed as described in the Click-iT Plus EdU Alexa Fluor 594 Imaging kit manual (Invitrogen).

Binucleation assay

DT40 cells were treated for 20 h with 0.2% EtOH (vol/vol) or 500 µM IAA. Cells were washed and resuspended in PBS, and allowed to adhere to poly-L-lysine–coated coverslips for 10 min. Cells were fixed in 3% paraformaldehyde in PBS for 10 min, then washed in PBS followed by permeabilization in 0.5% Triton X-100 in PBS for 20 min. Coverslips were mounted using mounting medium (4% *n*-propyl gallate, 80% glycerol, 20% PBS, and 1 µg/ml DAPI). Binucleated cells were scored based on DAPI staining.

Western blotting

For Western blot analysis, cells were lysed in RIPA buffer (1% NP-40, 0.5% sodium deoxycholate, 0.1% SDS, and protease inhibitor cocktail [Roche] in PBS) by syringing eight times through a 25 G needle. Lysates were cleared by centrifugation. Samples were separated on 9% polyacrylamide Tris-Glycine gels by SDS-PAGE. For analysis of TopBP1-YFP-AID, mouse anti-GFP monoclonal (Roche) and anti-mouse IgG conjugated to HRP (Dako) were used as primary and secondary antibodies, respectively. For analysis of CHK1-pS345, rabbit anti-phospho-CHK1 (Ser345; #2348; Cell Signaling), and anti–rabbit IgG conjugated to HRP (Dako) were used as primary and secondary antibodies, respectively.

Statistical methods

For microscopy experiments, the significance of the differences between cell populations was determined by a two-tailed unpaired *t* test. P-values were defined as significant if $P < 0.05$. Error bars representing 95% confidence intervals were calculated by Prism 6 (GraphPad Software). For mitotic timing of TopBP1-depleted cells, significance was tested by a Mann-Whitney test.

Online supplemental material

Fig. S1 shows a detailed analysis of TopBP1 colocalization with RPA and FANCD2. Fig. S2 shows a quantification of the origin of 53BP1 NBs. Fig. S3 shows localization of FANCD2 to sites of unscheduled DNA synthesis in mitosis. Fig. S4 shows a quantification of TopBP1 and SLX4 colocalization. Fig. S5 shows a quantification of colocalization of TopBP1 and EdU in mitosis with extended EdU incorporation. Table S1 lists the genotype and source of DT40 cell lines used in this study. Table S2 lists plasmids used in this study. Table S3 lists primers used in this study. Online supplemental material is available at http://www.jcb.org/cgi/content/full/jcb.201502107/DC1.

Acknowledgements

This work was supported by The Danish Agency for Science, Technology and Innovation, the Villum Kann Rasmussen Foundation, the Lundbeck Foundation, and the European Research Council (ERC) to M. Lisby; and the ERC to V.H. Oestergaard and R.T. Pedersen. J. Nilsson and T. Kruse were supported by a grant from the Novo Nordisk Foundation (NNF14CC0001) and the Danish Cancer Society.

The authors declare no competing financial interests.

Author contributions: R.T. Pedersen designed and performed most of the experiments, generated cell lines and constructs, analyzed data, and contributed to writing the paper. V.H. Oestergaard performed immunoblots, contributed to designing the experiments, conceived and supervised the project, and wrote the paper. J. Nilsson and T. Kruse performed all HeLa experiments. M. Lisby coordinated and supervised the project and contributed to writing the paper.

Submitted: 27 February 2015
Accepted: 9 July 2015

References

Arakawa, H., D. Lodygin, and J.M. Buerstedde. 2001. Mutant loxP vectors for selectable marker recycle and conditional knock-outs. *BMC Biotechnol.* 1:7. http://dx.doi.org/10.1186/1472-6750-1-7

Bai, L., W.M. Michael, and S. Yan. 2014. Importin β-dependent nuclear import of TopBP1 in ATR-Chk1 checkpoint in *Xenopus* egg extracts. *Cell. Signal.* 26:857–867. http://dx.doi.org/10.1016/j.cellsig.2014.01.006

Bartkova, J., Z. Horejsí, K. Koed, A. Krämer, F. Tort, K. Zieger, P. Guldberg, M. Sehested, J.M. Nesland, C. Lukas, et al. 2005. DNA damage response as a candidate anti-cancer barrier in early human tumorigenesis. *Nature.* 434:864–870. http://dx.doi.org/10.1038/nature03482

Baumann, C., R. Körner, K. Hofmann, and E.A. Nigg. 2007. PICH, a centromere-associated SNF2 family ATPase, is regulated by Plk1 and required for the spindle checkpoint. *Cell.* 128:101–114. http://dx.doi.org/10.1016/j.cell.2006.11.041

Bergoglio, V., A.S. Boyer, E. Walsh, V. Naim, G. Legube, M.Y. Lee, L. Rey, F. Rosselli, C. Cazaux, K.A. Eckert, and J.S. Hoffmann. 2013. DNA synthesis by Pol η promotes fragile site stability by preventing under-replicated DNA in mitosis. *J. Cell Biol.* 201:395–408. http://dx.doi.org/10.1083/jcb.201207066

Beroukhim, R., C.H. Mermel, D. Porter, G. Wei, S. Raychaudhuri, J. Donovan, J. Barretina, J.S. Boehm, J. Dobson, M. Urashima, et al. 2010. The landscape of somatic copy-number alteration across human cancers. *Nature.* 463:899–905. http://dx.doi.org/10.1038/nature08822

Bhat, A., P.L. Andersen, Z. Qin, and W. Xiao. 2013. Rev3, the catalytic subunit of Polζ, is required for maintaining fragile site stability in human cells. *Nucleic Acids Res.* 41:2328–2339. http://dx.doi.org/10.1093/nar/gks1442

Bignell, G.R., C.D. Greenman, H. Davies, A.P. Butler, S. Edkins, J.M. Andrews, G. Buck, L. Chen, D. Beare, C. Latimer, et al. 2010. Signatures of mutation and selection in the cancer genome. *Nature.* 463:893–898. http://dx.doi.org/10.1038/nature08768

Brandao, G.C., G.D. Matos, R.N. Pereira, and S.L. Ferreira. 2014. Development of a simple method for the determination of nitrite and nitrate in groundwater by high-resolution continuum source electrothermal molecular absorption spectrometry. *Anal. Chim. Acta.* 806:101–106. http://dx.doi.org/10.1016/j.aca.2013.11.031

Cescutti, R., S. Negrini, M. Kohzaki, and T.D. Halazonetis. 2010. TopBP1 functions with 53BP1 in the G1 DNA damage checkpoint. *EMBO J.* 29:3723–3732. http://dx.doi.org/10.1038/emboj.2010.238

Chan, K.L., P.S. North, and I.D. Hickson. 2007. BLM is required for faithful chromosome segregation and its localization defines a class of ultrafine anaphase bridges. *EMBO J.* 26:3397–3409. http://dx.doi.org/10.1038/sj.emboj.7601777

Chan, K.L., T. Palmai-Pallag, S. Ying, and I.D. Hickson. 2009. Replication stress induces sister-chromatid bridging at fragile site loci in mitosis. *Nat. Cell Biol.* 11:753–760. http://dx.doi.org/10.1038/ncb1882

Cormack, B.P., R.H. Valdivia, and S. Falkow. 1996. FACS-optimized mutants of the green fluorescent protein (GFP). *Gene.* 173:33–38. http://dx.doi.org/10.1016/0378-1119(95)00685-0

Durkin, S.G., and T.W. Glover. 2007. Chromosome fragile sites. *Annu. Rev. Genet.* 41:169–192. http://dx.doi.org/10.1146/annurev.genet.41.042007.165900

Eykelenboom, J.K., E.C. Harte, L. Canavan, A. Pastor-Peidro, I. Calvo-Asensio, M. Llorens-Agost, and N.F. Lowndes. 2013. ATR activates the S-M checkpoint during unperturbed growth to ensure sufficient replication prior to mitotic onset. *Cell Reports.* 5:1095–1107. http://dx.doi.org/10.1016/j.celrep.2013.10.027

Fekairi, S., S. Scaglione, C. Chahwan, E.R. Taylor, A. Tissier, S. Coulon, M.Q. Dong, C. Ruse, J.R. Yates III, P. Russell, et al. 2009. Human SLX4 is a Holliday junction resolvase subunit that binds multiple DNA repair/recombination endonucleases. *Cell.* 138:78–89. http://dx.doi.org/10.1016/j.cell.2009.06.029

Gallo-Fernández, M., I. Saugar, M.A. Ortiz-Bazán, M.V. Vázquez, and J.A. Tercero. 2012. Cell cycle-dependent regulation of the nuclease activity of Mus81-Eme1/Mms4. *Nucleic Acids Res.* 40:8325–8335. http://dx.doi.org/10.1093/nar/gks599

Germann, S.M., V.H. Oestergaard, C. Haas, P. Salis, A. Motegi, and M. Lisby. 2011. Dpb11/TopBP1 plays distinct roles in DNA replication, checkpoint response and homologous recombination. *DNA Repair (Amst.).* 10:210–224. http://dx.doi.org/10.1016/j.dnarep.2010.11.001

Germann, S.M., V. Schramke, R.T. Pedersen, I. Gallina, N. Eckert-Boulet, V.H. Oestergaard, and M. Lisby. 2014. TopBP1/Dpb11 binds DNA anaphase bridges to prevent genome instability. *J. Cell Biol.* 204:45–59. http://dx.doi.org/10.1083/jcb.201305157

Germe, T., and O. Hyrien. 2005. Topoisomerase II-DNA complexes trapped by ICRF-193 perturb chromatin structure. *EMBO Rep.* 6:729–735. http://dx.doi.org/10.1038/sj.embor.7400465

Goedhart, J., L. van Weeren, M.A. Hink, N.O. Vischer, K. Jalink, and T.W. Gadella Jr. 2010. Bright cyan fluorescent protein variants identified by fluorescence lifetime screening. *Nat. Methods.* 7:137–139. http://dx.doi.org/10.1038/nmeth.1415

Gritenaite, D., L.N. Princz, B. Szakal, S.C. Bantele, L. Wendeler, S. Schilbach, B.H. Habermann, J. Matos, M. Lisby, D. Branzei, and B. Pfander. 2014. A cell cycle-regulated Slx4-Dpb11 complex promotes the resolution of DNA repair intermediates linked to stalled replication. *Genes Dev.* 28:1604–1619. http://dx.doi.org/10.1101/gad.240515.114

Guervilly, J.H., A. Takedachi, V. Naim, S. Scaglione, C. Chawhan, Y. Lovera, E. Despras, I. Kuraoka, P. Kannouche, F. Rosselli, and P.H. Gaillard. 2015. The SLX4 complex is a SUMO E3 ligase that impacts on replication stress outcome and genome stability. *Mol. Cell.* 57:123–137. http://dx.doi.org/10.1016/j.molcel.2014.11.014

Guo, Z., A. Kumagai, S.X. Wang, and W.G. Dunphy. 2000. Requirement for Atr in phosphorylation of Chk1 and cell cycle regulation in response to DNA replication blocks and UV-damaged DNA in *Xenopus* egg extracts. *Genes Dev.* 14:2745–2756. http://dx.doi.org/10.1101/gad.842500

Halazonetis, T.D., V.G. Gorgoulis, and J. Bartek. 2008. An oncogene-induced DNA damage model for cancer development. *Science.* 319:1352–1355. http://dx.doi.org/10.1126/science.1140735

Harrigan, J.A., R. Belotserkovskaya, J. Coates, D.S. Dimitrova, S.E. Polo, C.R. Bradshaw, P. Fraser, and S.P. Jackson. 2011. Replication stress induces 53BP1-containing OPT domains in G1 cells. *J. Cell Biol.* 193:97–108. http://dx.doi.org/10.1083/jcb.201011083

Johnson, M., H.H. Phua, S.C. Bennett, J.M. Spence, and C.J. Farr. 2009. Studying vertebrate topoisomerase 2 function using a conditional knockdown system in DT40 cells. *Nucleic Acids Res.* 37:e98. http://dx.doi.org/10.1093/nar/gkp480

Kim, J.E., S.A. McAvoy, D.I. Smith, and J. Chen. 2005. Human TopBP1 ensures genome integrity during normal S phase. *Mol. Cell. Biol.* 25:10907–10915. http://dx.doi.org/10.1128/MCB.25.24.10907-10915.2005

Kruse, T., G. Zhang, M.S. Larsen, T. Lischetti, W. Streicher, T. Kragh Nielsen, S.P. Bjørn, and J. Nilsson. 2013. Direct binding between BubR1 and B56-PP2A phosphatase complexes regulate mitotic progression. *J. Cell Sci.* 126:1086–1092. http://dx.doi.org/10.1242/jcs.122481

Kumagai, A., J. Lee, H.Y. Yoo, and W.G. Dunphy. 2006. TopBP1 activates the ATR-ATRIP complex. *Cell.* 124:943–955. http://dx.doi.org/10.1016/j.cell.2005.12.041

Le Beau, M.M., F.V. Rassool, M.E. Neilly, R. Espinosa III, T.W. Glover, D.I. Smith, and T.W. McKeithan. 1998. Replication of a common fragile site, FRA3B, occurs late in S phase and is delayed further upon induction: implications for the mechanism of fragile site induction. *Hum. Mol. Genet.* 7:755–761. http://dx.doi.org/10.1093/hmg/7.4.755

Lee, D.H., S.S. Acharya, M. Kwon, P. Drane, Y. Guan, G. Adelmant, P. Kalev, J. Shah, D. Pellman, J.A. Marto, and D. Chowdhury. 2014. Dephosphorylation enables the recruitment of 53BP1 to double-strand DNA breaks. *Mol. Cell.* 54:512–525. http://dx.doi.org/10.1016/j.molcel.2014.03.020

Le Tallec, B., G.A. Millot, M.E. Blin, O. Brison, B. Dutrillaux, and M. Debatisse. 2013. Common fragile site profiling in epithelial and erythroid cells reveals that most recurrent cancer deletions lie in fragile sites hosting large genes. *Cell Reports.* 4:420–428. http://dx.doi.org/10.1016/j.celrep.2013.07.003

Liu, K., J.D. Graves, J.D. Scott, R. Li, and W.C. Lin. 2013. Akt switches TopBP1 function from checkpoint activation to transcriptional regulation through phosphoserine binding-mediated oligomerization. *Mol. Cell. Biol.* 33:4685–4700. http://dx.doi.org/10.1128/MCB.00373-13

Lukas, C., V. Savic, S. Bekker-Jensen, C. Doil, B. Neumann, R.S. Pedersen, M. Grøfte, K.L. Chan, I.D. Hickson, J. Bartek, and J. Lukas. 2011. 53BP1 nuclear bodies form around DNA lesions generated by mitotic transmission of chromosomes under replication stress. *Nat. Cell Biol.* 13:243–253. http://dx.doi.org/10.1038/ncb2201

Mäkiniemi, M., T. Hillukkala, J. Tuusa, K. Reini, M. Vaara, D. Huang, H. Pospiech, I. Majuri, T. Westerling, T.P. Mäkelä, and J.E. Syväoja. 2001. BRCT domain-containing protein TopBP1 functions in DNA replication and damage response. *J. Biol. Chem.* 276:30399–30406. http://dx.doi.org/10.1074/jbc.M102245200

Matos, J., M.G. Blanco, S. Maslen, J.M. Skehel, and S.C. West. 2011. Regulatory control of the resolution of DNA recombination intermediates during meiosis and mitosis. *Cell.* 147:158–172. http://dx.doi.org/10.1016/j.cell.2011.08.032

Matos, J., M.G. Blanco, and S.C. West. 2013. Cell-cycle kinases coordinate the resolution of recombination intermediates with chromosome segregation. *Cell Reports.* 4:76–86. http://dx.doi.org/10.1016/j.celrep.2013.05.039

Muñoz, I.M., K. Hain, A.C. Déclais, M. Gardiner, G.W. Toh, L. Sanchez-Pulido, J.M. Heuckmann, R. Toth, T. Macartney, B. Eppink, et al. 2009. Coordination of structure-specific nucleases by human SLX4/BTBD12 is required for DNA repair. *Mol. Cell.* 35:116–127. http://dx.doi.org/10.1016/j.molcel.2009.06.020

Nagai, T., K. Ibata, E.S. Park, M. Kubota, K. Mikoshiba, and A. Miyawaki. 2002. A variant of yellow fluorescent protein with fast and efficient maturation for cell-biological applications. *Nat. Biotechnol.* 20:87–90. http://dx.doi.org/10.1038/nbt0102-87

Naim, V., and F. Rosselli. 2009. The FANC pathway and BLM collaborate during mitosis to prevent micro-nucleation and chromosome abnormalities. *Nat. Cell Biol.* 11:761–768. http://dx.doi.org/10.1038/ncb1883

Naim, V., T. Wilhelm, M. Debatisse, and F. Rosselli. 2013. ERCC1 and MUS81-EME1 promote sister chromatid separation by processing late replication intermediates at common fragile sites during mitosis. *Nat. Cell Biol.* 15:1008–1015. http://dx.doi.org/10.1038/ncb2793

Nishimura, K., T. Fukagawa, H. Takisawa, T. Kakimoto, and M. Kanemaki. 2009. An auxin-based degron system for the rapid depletion of proteins in nonplant cells. *Nat. Methods.* 6:917–922. http://dx.doi.org/10.1038/nmeth.1401

Oestergaard, V.H., B.R. Knudsen, and A.H. Andersen. 2004. Dissecting the cell-killing mechanism of the topoisomerase II-targeting drug ICRF-193. *J. Biol. Chem.* 279:28100–28105. http://dx.doi.org/10.1074/jbc.M402119200

Oestergaard, V.H., C. Pentzold, R.T. Pedersen, S. Iosif, A. Alpi, S. Bekker-Jensen, N. Mailand, and M. Lisby. 2012. RNF8 and RNF168 but not HERC2 are required for DNA damage-induced ubiquitylation in chicken DT40 cells. *DNA Repair (Amst.).* 11:892–905. http://dx.doi.org/10.1016/j.dnarep.2012.08.005

Ohouo, P.Y., F.M. Bastos de Oliveira, B.S. Almeida, and M.B. Smolka. 2010. DNA damage signaling recruits the Rtt107-Slx4 scaffolds via Dpb11 to mediate replication stress response. *Mol. Cell.* 39:300–306. http://dx.doi.org/10.1016/j.molcel.2010.06.019

Oliveira, R.A., R.S. Hamilton, A. Pauli, I. Davis, and K. Nasmyth. 2010. Cohesin cleavage and Cdk inhibition trigger formation of daughter nuclei. *Nat. Cell Biol.* 12:185–192. http://dx.doi.org/10.1038/ncb2018

Orthwein, A., A. Fradet-Turcotte, S.M. Noordermeer, M.D. Canny, C.M. Brun, J. Strecker, C. Escribano-Diaz, and D. Durocher. 2014. Mitosis inhibits DNA double-strand break repair to guard against telomere fusions. *Science.* 344:189–193. http://dx.doi.org/10.1126/science.1248024

Ouyang, J., E. Garner, A. Hallet, H.D. Nguyen, K.A. Rickman, G. Gill, A. Smogorzewska, and L. Zou. 2015. Noncovalent interactions with

SUMO and ubiquitin orchestrate distinct functions of the SLX4 complex in genome maintenance. *Mol. Cell.* 57:108–122. http://dx.doi.org/10.1016/j.molcel.2014.11.015

Petermann, E., and T. Helleday. 2010. Pathways of mammalian replication fork restart. *Nat. Rev. Mol. Cell Biol.* 11:683–687. http://dx.doi.org/10.1038/nrm2974

Reini, K., L. Uitto, D. Perera, P.B. Moens, R. Freire, and J.E. Syväoja. 2004. TopBP1 localises to centrosomes in mitosis and to chromosome cores in meiosis. *Chromosoma.* 112:323–330. http://dx.doi.org/10.1007/s00412-004-0277-5

Roca, J., R. Ishida, J.M. Berger, T. Andoh, and J.C. Wang. 1994. Antitumor bisdioxopiperazines inhibit yeast DNA topoisomerase II by trapping the enzyme in the form of a closed protein clamp. *Proc. Natl. Acad. Sci. USA.* 91:1781–1785. http://dx.doi.org/10.1073/pnas.91.5.1781

Rouse, J. 2004. Esc4p, a new target of Mec1p (ATR), promotes resumption of DNA synthesis after DNA damage. *EMBO J.* 23:1188–1197. http://dx.doi.org/10.1038/sj.emboj.7600129

Samejima, K., I. Samejima, P. Vagnarelli, H. Ogawa, G. Vargiu, D.A. Kelly, F. de Lima Alves, A. Kerr, L.C. Green, D.F. Hudson, et al. 2012. Mitotic chromosomes are compacted laterally by KIF4 and condensin and axially by topoisomerase IIα. *J. Cell Biol.* 199:755–770. http://dx.doi.org/10.1083/jcb.201202155

Shaner, N.C., R.E. Campbell, P.A. Steinbach, B.N. Giepmans, A.E. Palmer, and R.Y. Tsien. 2004. Improved monomeric red, orange and yellow fluorescent proteins derived from *Discosoma* sp. red fluorescent protein. *Nat. Biotechnol.* 22:1567–1572. http://dx.doi.org/10.1038/nbt1037

Svendsen, J.M., A. Smogorzewska, M.E. Sowa, B.C. O'Connell, S.P. Gygi, S.J. Elledge, and J.W. Harper. 2009. Mammalian BTBD12/SLX4 assembles a Holliday junction resolvase and is required for DNA repair. *Cell.* 138:63–77. http://dx.doi.org/10.1016/j.cell.2009.06.030

Szakal, B., and D. Branzei. 2013. Premature Cdk1/Cdc5/Mus81 pathway activation induces aberrant replication and deleterious crossover. *EMBO J.* 32:1155–1167. http://dx.doi.org/10.1038/emboj.2013.67

Toledo, L.I., M. Murga, R. Zur, R. Soria, A. Rodriguez, S. Martinez, J. Oyarzabal, J. Pastor, J.R. Bischoff, and O. Fernandez-Capetillo. 2011. A cell-based screen identifies ATR inhibitors with synthetic lethal properties for cancer-associated mutations. *Nat. Struct. Mol. Biol.* 18:721–727. http://dx.doi.org/10.1038/nsmb.2076

Uhlmann, F., D. Wernic, M.A. Poupart, E.V. Koonin, and K. Nasmyth. 2000. Cleavage of cohesin by the CD clan protease separin triggers anaphase in yeast. *Cell.* 103:375–386. http://dx.doi.org/10.1016/S0092-8674(00)00130-6

Van Hatten, R.A., A.V. Tutter, A.H. Holway, A.M. Khederian, J.C. Walter, and W.M. Michael. 2002. The *Xenopus* Xmus101 protein is required for the recruitment of Cdc45 to origins of DNA replication. *J. Cell Biol.* 159:541–547. http://dx.doi.org/10.1083/jcb.200207090

Wang, J., J. Chen, and Z. Gong. 2013. TopBP1 controls BLM protein level to maintain genome stability. *Mol. Cell.* 52:667–678. http://dx.doi.org/10.1016/j.molcel.2013.10.012

Wyatt, H.D., S. Sarbajna, J. Matos, and S.C. West. 2013. Coordinated actions of SLX1-SLX4 and MUS81-EME1 for Holliday junction resolution in human cells. *Mol. Cell.* 52:234–247. http://dx.doi.org/10.1016/j.molcel.2013.08.035

Yamamoto, K.N., S. Kobayashi, M. Tsuda, H. Kurumizaka, M. Takata, K. Kono, J. Jiricny, S. Takeda, and K. Hirota. 2011. Involvement of SLX4 in interstrand cross-link repair is regulated by the Fanconi anemia pathway. *Proc. Natl. Acad. Sci. USA.* 108:6492–6496. http://dx.doi.org/10.1073/pnas.1018487108

Yamane, K., M. Kawabata, and T. Tsuruo. 1997. A DNA-topoisomerase-II-binding protein with eight repeating regions similar to DNA-repair enzymes and to a cell-cycle regulator. *Eur. J. Biochem.* 250:794–799. http://dx.doi.org/10.1111/j.1432-1033.1997.00794.x

Yamane, K., J. Chen, and T.J. Kinsella. 2003. Both DNA topoisomerase II-binding protein 1 and BRCA1 regulate the G2-M cell cycle checkpoint. *Cancer Res.* 63:3049–3053.